AD-A172 025 LIFE PREDICTION OF TURBINE BLADE NICKEL BASE SUPERALLOY 1/1
SINGLE CRYSTALS(U) UNIVERSAL ENERGY SYSTEMS INC DAYTON
OH Y SRINIVASAN AUG 86 AFWAL-TR-86-4045
UNCLASSIFIED F33615-83-C-5119 F/G 11/6 NL

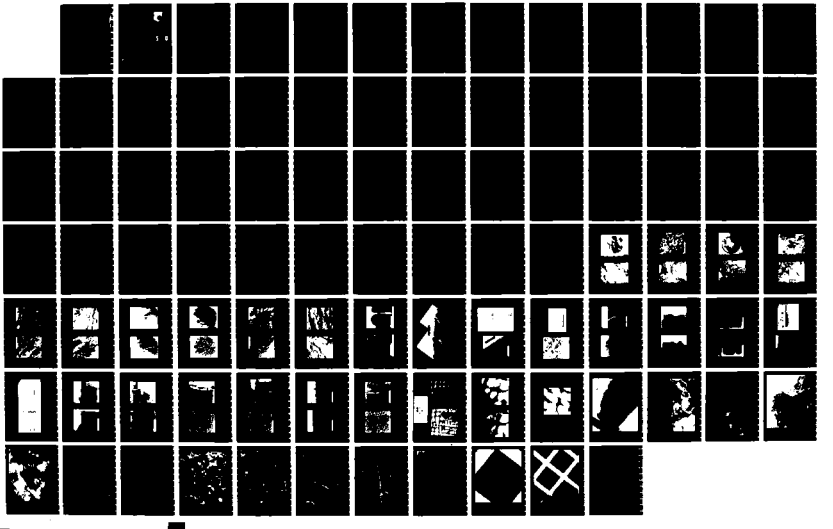

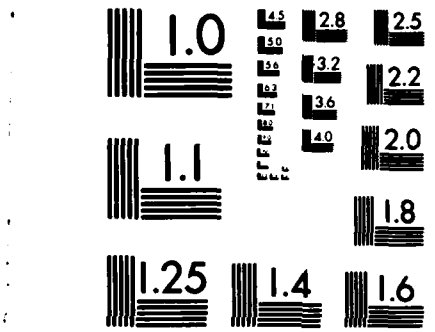
1.0
1.1
1.25
1.4
1.6
1.8
2.0
2.2
2.5
2.8
3.2
3.6
4.0
4.5
5.0
5.6
6.3
7.1
8.0
9.0
10.0

(2)

AFWAL-TR-86-4045

# LIFE PREDICTION OF TURBINE BLADE NICKEL BASE SUPERALLOY SINGLE CRYSTALS

Dr. V. Srinivasan

Universal Energy Systems, Inc.
4401 Dayton-Xenia Road
Dayton, Ohio 45432

AD-A172 025

August 1986

Final Report for Period 1 October 1983 - 31 March 1984

DTIC
ELECTE
SEP 17 1986
S D
D

Approved for Public Release; Distribution is Unlimited

DTIC FILE COPY

MATERIALS LABORATORY
AIR FORCE WRIGHT AERONAUTICAL LABORATORIES
AIR FORCE SYSTEMS COMMAND
WRIGHT-PATTERSON AIR FORCE BASE, OHIO 45433-6533

86 9 16 055

ASD 86 1786

*NOTICE*

*When Government drawings, specifications, or other data are used for any purpose other than in connection with a definitely related Government procurement operation, the United States Government thereby incurs no responsibility nor any obligation whatsoever; and the fact that the government may have formulated, furnished, or in any way supplied the said drawings, specifications, or other data, is not to be regarded by implication or otherwise as in any manner licensing the holder or any other person or corporation, or conveying any rights or permission to manufacture use, or sell any patented invention that may in any way be related thereto.*

*This report has been reviewed by the Office of Public Affairs (ASD/PA) and is releasable to the National Technical Information Service (NTIS). At NTIS, it will be available to the general public, including foreign nations.*

*This technical report has been reviewed and is approved for publication.*

JOHN P. HENDERSON, Chief
Metals Behavior Branch
Metals and Ceramics Division

BRYAN H. FORTSON, 1Lt, USAF
Project Engineer
Metals Behavior Branch

FOR THE COMMANDER:

LAWRENCE N. HJELM, Asst Chief
Metals and Ceramics Division
Materials Laboratory

*If your address has changed, if you wish to be removed from our mailing list, or if the addressee is no longer employed by your organization please notify* AFWAL/MLLN, *W-PAFB, OH 45433 to help us maintain a current mailing list.*

*Copies of this report should not be returned unless return is required by security considerations, contractual obligations, or notice on a specific document.*

Unclassified

SECURITY CLASSIFICATION OF THIS PAGE

## REPORT DOCUMENTATION PAGE

| | |
|---|---|
| 1a. REPORT SECURITY CLASSIFICATION: Unclassified | 1b. RESTRICTIVE MARKINGS: AD-A172 025 |
| 2a. SECURITY CLASSIFICATION AUTHORITY | 3. DISTRIBUTION/AVAILABILITY OF REPORT: Approved for Public Release; Distribution is Unlimited |
| 2b. DECLASSIFICATION/DOWNGRADING SCHEDULE | |
| 4. PERFORMING ORGANIZATION REPORT NUMBER(S) | 5. MONITORING ORGANIZATION REPORT NUMBER(S): AFWAL-TR-86-4045 |
| 6a. NAME OF PERFORMING ORGANIZATION: Universal Energy Systems, Inc. / 6b. OFFICE SYMBOL (If applicable) | 7a. NAME OF MONITORING ORGANIZATION: Materials Laboratory, Air Force Wright Aeronautical Laboratories |
| 6c. ADDRESS (City, State and ZIP Code): 4401 Dayton-Xenia Road, Dayton, OH 45432 | 7b. ADDRESS (City, State and ZIP Code): Wright-Patterson AFB, OH 45433-6533 |
| 8a. NAME OF FUNDING/SPONSORING ORGANIZATION / 8b. OFFICE SYMBOL (If applicable): AFWAL/MLLN | 9. PROCUREMENT INSTRUMENT IDENTIFICATION NUMBER: F33615-83-C-5119 |
| 8c. ADDRESS (City, State and ZIP Code): Wright-Patterson AFB, OH 45433-6533 | 10. SOURCE OF FUNDING NOS. |

| PROGRAM ELEMENT NO. | PROJECT NO. | TASK NO. | WORK UNIT NO. |
|---|---|---|---|
| 65502F | 3005 | 50 | 08 |

11. TITLE (Include Security Classification): Life Prediction of Turbine Blade Nickel Base Superalloy Single Crystals (uncl.)

12. PERSONAL AUTHOR(S): Srinivasan, V.

| 13a. TYPE OF REPORT | 13b. TIME COVERED | 14. DATE OF REPORT (Yr., Mo., Day) | 15. PAGE COUNT |
|---|---|---|---|
| Summary | FROM 1 Oct 83 TO 31Mar84 | August 1986 | 89 |

16. SUPPLEMENTARY NOTATION: Small Business Innovation Research Report.

| 17. COSATI CODES | | | 18. SUBJECT TERMS (Continue on reverse if necessary and identify by block number) |
|---|---|---|---|
| FIELD | GROUP | SUB. GR. | superalloys, single crystals, fatigue, microstructures, fracture |
| 11 | 06 | | |
| | | | |

19. ABSTRACT (Continue on reverse if necessary and identify by block number): The result of Phase I research is reported along with a brief discussion on the technical feasibility of the approach. The objective of this research is to develop life prediction method for single crystal Rene N4+ through mechanistic and microstructural approaches. LCF tests were performed at 1093°C. The effect of three strain ranges, hold-time and coating were considered. Surface replicas were taken in the early part of the tests. Fracture surfaces, longitudinal sections and thin foils were examined using SEM, TEM, and EDAX techniques. The precipitates γ' coarsened during the test. There was an increase in the tensile mean stress. In all specimens almost cracks were surface-nucleated. While the micropores appear to be the nucleation sites in the uncoated sample, the nature of nucleation sites on the coating surfaces is not clear. Transverse cracks along the gage, and several secondary cracks below the fracture surfaces were observed. Oxides covered the fracture surfaces. Coatings did not affect the LCF lives. The LCF lives followed a linear relation between strain range and cycles to failure.

(CONTINUED)

| 20. DISTRIBUTION/AVAILABILITY OF ABSTRACT | 21. ABSTRACT SECURITY CLASSIFICATION |
|---|---|
| UNCLASSIFIED/UNLIMITED ☐ SAME AS RPT. ☐ DTIC USERS ☐ | Unclassified |

| 22a. NAME OF RESPONSIBLE INDIVIDUAL | 22b. TELEPHONE NUMBER (Include Area Code) | 22c. OFFICE SYMBOL |
|---|---|---|
| Lt Bryan H. Fortson | (513) 255-2689 | AFWAL/MLLN |

DD FORM 1473, 83 APR — EDITION OF 1 JAN 73 IS OBSOLETE.

Unclassified

SECURITY CLASSIFICATION OF THIS PAGE

CONTINUATION - Block 19.

The Phase I results and the results of Phase II (if funded) will have immediate application in the component retirement programs of the U.S. Air Force and Navair, and in the alloy development programs of General Electric Co., Cincinnati, OH.

QUALITY INSPECTED 8

Accesion For
NTIS CRA&I
DTIC TAB
Unannounced
Justification
By
Distribution /
Availability Codes
Dist | Avail and / or Special
A-1

TABLE OF CONTENTS


| SECTION | | | PAGE |
|---|---|---|---|
| 1.0 | | INTRODUCTION | 1 |
| 2.0 | | TECHNICAL OBJECTIVES | 4 |
| 3.0 | | EXPERIMENTAL ALLOY AND METHOD | 5 |
| | 3.1 | Experimental Alloy | 5 |
| | 3.2 | High Temperature Low Cycle Fatigue Test | 5 |
| | 3.3 | Microstructural Examination | 7 |
| 4.0 | | RESULTS AND DISCUSSION | 9 |
| | 4.1 | Mechanical Test Results | 9 |
| | 4.2 | Metallography Results | 10 |
| | 4.3 | Discussion | 16 |
| 5.0 | | CONCLUSIONS | 19 |
| 6.0 | | ESTIMATE OF TECHNICAL FEASIBILITY | 20 |
| | | REFERENCES | 22 |
| | | TABLES | 24 |
| | | FIGURES | 28 |

# LIST OF TABLES


| TABLE | | PAGE |
|---|---|---|
| I | Nominal Chemical Composition of René N4, Wt. % | 24 |
| II | Orientation of Cast Direction with respect to [001] | 25 |
| III | Test Matrix | 26 |
| IV | LCF Data Summary for René N4+ | 27 |

LIST OF ILLUSTRATIONS


| FIGURE | | PAGE |
|---|---|---|
| 1. | LCF HCF Specimen Dimensions | 28 |
| 2. | LCF Wave Forms Used | 29 |
| 3. | The Relationship between the Total Strain Range, $\Delta\varepsilon_t$ and the Number of cycles to Failure, in uncoated Rene' N4+ | 30 |
| 4. | The Relationship between the Total Strain Range, $\Delta\varepsilon_t$ and the Number of cycles to Failure, in the Codep-Coated René N4+ | 31 |
| 5. | The Relationship between the Total Strain Range, $\Delta\varepsilon_t$ and the Number of Cycles to Failure, in the PS6MY Coated René N4+ | 32 |
| 6. | Comparison of LCF Data obtained on the bare-, the Codep-Coated and the PS6MY Coated René N4+ | 33 |
| 7. | Relationships between the Total Strain Range and Time to Failure for the Uncoated and coated René N4+ | 34 |
| 8. | Hysteresis Loops, (Bare K 149 - 2) $\Delta\varepsilon_t$ = 0.35% | 35 |
| 9. | Hysteresis Loops, (Bare J 149 - 1) | 36 |
| 10. | Fracture Surfaces of Bare L 151 - 1, $\Delta\varepsilon_t$ = 0.6%, Continuous Cycling at 1093°C (2000°F) | 38 |
| 11. | Fracture Surfaces of Bare L 151 - 1, $\Delta\varepsilon_t$ = 0.6%, $N_f$ = 4,956 cy. Continuous Cycling at 1093°C (2000°F) | 39 |
| 12. | Fracture Surfaces of Bare E 151 - 2, $\Delta\varepsilon_t$ = 0.6%, $N_f$ = 1,755 cy. Test with a 2 min. Hold in Compression at 1093°C (2000°F) | 40 |
| 13. | Fracture Surfaces of Bare E 151 - 2, $\Delta\varepsilon_t$ = 0.6%, $N_f$ = 1,755 cy. Test with a 2 min. Hold in Compression at 1093°C (2000°F) | 41 |
| 14. | Fracture surfaces of Codep coated L 151 - 4 - C1, $\Delta\varepsilon_t$ = 0.6%, $N_f$ = 1,708 cy. Test with a 2 min. Hold in Compression at 1093°C (2000°F) | 42 |
| 15. | Room Temperature Fracture Regions in the Codep-Coated L 151 - 4 - C1. Note Microvoid Coalescence, Casting Micropores and Coating Decohesion | 43 |

LIST OF ILLUSTRATIONS (con't)


| FIGURE | | PAGE |
|---|---|---|
| 16. | Fracture Surfaces of Codep-Coated K 149 - 3 - C1, $\Delta\varepsilon_t$ = 0.45%, $N_f$ = 3,693 cy. Test with a 2 min. Hold in Compression at 1093°C (2000°F) | 44 |
| 17. | Fracture Surfaces of Codep-Coated K 149 - 3 - C1 covered with oxides, $\Delta\varepsilon_t$ = 0.45%, $N_f$ = 3,693 cy. Test with a 2 min. Hold in Compression at 1093°C (2000°F) | 45 |
| 18. | Fracture Surfaces of Codep-Coated J 149 - 4 - C1 covered with oxides, $\Delta\varepsilon_t$ = 0.35%, $N_f$ = 26,330 cy. Continuous Cycling at 1093°C (2000°F) | 46 |
| 19. | Fracture Surfaces of Codep-Coated E 151 - 3 - C1, $\Delta\varepsilon_t$ = 0.35%, $N_f$ = 26,330 cy. Continuous cycling at 1093°C (2000°F) | 47 |
| 20. | Longitudinal Sections of Uncoated K 149 - 2; Transverse Cracks and changes in the Precipitates Morphology after Continuous LCF Test at $\Delta\varepsilon_t$ = 0.35%, $N_f$ = 18,983 cy. at 1093°C (2000°F) | 48 |
| 21. | Longitudinal Sections of Uncoated L 151 - 1 Near the Fracture Region with Several Subfracture Surface cracks, Test condition: Continuous Cycling, $\Delta\varepsilon_t$ = 0.35%, $N_f$ = 4,965 cy. T = 1093°C (2000°F) | 49 |
| 22. | (a) Longitudinal Section of Uncoated L 151 - 1 showing the Oxidized Edge; $\Delta\varepsilon_t$ = 0.6%, $N_f$ 4,965 cy. Continuous Cycling, T = 1093°C (2000°F), (b) EDAX Spectra from the Interior, (c) from the Oxidized Edge | 50 |
| 23. | (a) Longitudinal Section of uncoated L 151 - 1 with Inclusions, (b) EDAX Spectrum of an Inclusion | 51 |
| 24. | Longitudinal Sections of Uncoated L 151 - 1 with Transverse Cracks originating from the Free Surface. Continuous Cycling at $\Delta\varepsilon_t$ = 0.6%, $N_f$ 4,965 cy, T = 1093°C (2000°F) | 52 |
| 25. | Longitudinal Sections of Uncoated E151-2 Near the Fracture Region Showing Many Surface-connected Secondary Cracks Below the Fracture Surface, $\Delta\varepsilon_t$ = 0.6%, $N_f$ = 1,755 cy, T = 1093°C (2000°F), Test with a 2 min. Hold in Compression | 53 |
| 26. | Longitudinal Sections of Uncoated E 151 - 2 with many Transverse Cracks originating from the Surface Test Conditions; $\Delta\varepsilon_t$ = 0.6%, T = 1093°C (2000°F), 2 min. Compression Hold, $N_f$ = 1,755 cy. | 54 |

| FIGURE | | PAGE |
|---|---|---|
| 27. | (a) Longitudinal Section of Codep-Coated J 149 - 4 - C1 showing Transverse Cracks after Continuous Cycling with $\Delta\varepsilon_t$ = 0.35% at 1093°C (2000°F), and $N_f$ = 26,330 cy. (b) Change in the Precipitate Morphology. | 55 |
| 28. | EDAX Spectra (a) from the Outer Region in the Codep-Coating, (b) from the Diffusion Zone and (c) from the Substrate J 149 - 4 - C1. After Continuous Cycling Test with $\Delta\varepsilon_t$ = 0.35% at 1093°C (2000°F) and $N_f$ = 26,330 cy. | 56 |
| 29. | Longitudinal Sections of Codep-Coated J 149 - 4 - C1 with Subfracture Surface Cracks Test Conditions; $\Delta\varepsilon_t$ = 0.35%, Continuous Cycling, T = 1093°C (2000°F) and $N_f$ = 26,330 cy. | 57 |
| 30. | Longitudinal Sections of Codep-Coated E 151 - 3 - C1 with Transverse Cracks Test Condtions; $\Delta\varepsilon_t$ = 0.35%, T = 1093°C (2000°F), 2 min. Hold in Compression, $N_f$ = 5,311 cy. | 58 |
| 31. | (a) Longitudinal Section showing Subfracture Surface Cracks in the Codep-Coated E 151 - 3 - C1, (b) changes in the Precipitate Morphology. Test Conditions; $\Delta\varepsilon_t$ = 0.35%, T = 1093°C (2000°F), 2 min. Hold in Compression, $N_f$ = 5,311 cy. | 59 |
| 32. | (a) Longitudinal Section showing a Transverse Crack in the PS6MY-Coated L 171 - 1 C2, (b) changes in the Precipitate Morphology Test Conditions; $\Delta\varepsilon_t$ = 0.35%, T = 1093°C (2000°F), Continuous Cycling, $N_f$ = 16,072 cy. | 60 |
| 33. | Longitudinal Sections of PS6MY-Coated L 171 - 2 - C2 with several Transverse Cracks, Test Conditions: $\Delta\varepsilon_t$ 0.35%, T=1093°C(2000°F), 2 min. Compression Hold, $N_f$= 5,149 cy. | 61 |
| 34. | (a) Longitudinal Section of PS6MY-Coated L 171 - 2 - C2 Showing a Segment of a Long Crack. (b) Change in the Precipitate Morpholopy, Test Conditions: $\Delta\varepsilon_t$ =0.35%, T=1093°C (2000°F), 2 min. Compression Hold, $N_f$ = 5,149 cy. | 62 |
| 35. | Pretest Microstructure. (a) Electron Diffraction Pattern, Zone Orientation B=[100], (b) Bright Field Image, (c) Dark Field Image of Same Area as in (b) With the Precipitate Diffraction Spot, 200. | 63 |
| 36. | Transmission Electron Micrograph of as heat treated René N4+ (a) with g = 200 (b) with g = 220 | 64 |

LIST OF ILLUSTRATIONS (con't)


| FIGURE | | PAGE |
|---|---|---|
| 37 | Transmission Electron Micrograph of as heat treated René N4+ obtained with g = 020. | 65 |
| 38 | Transmission Electron Micrograph of Uncoated K 149 - 2 Showing Interfacial Dislocations, 75,000X. Test Conditions: $\Delta\varepsilon_t$ = 0.35%, T = 1093°C(2000°F), Continuous Cycling, $N_f$ = 8,983 cy. | 66 |
| 39 | Transmission Electron Micrograph of Uncoated L 151 - 1 Showing Interfacial Dislocations, 75,000X. Test Conditions: $\Delta\varepsilon_t$ = 0.6%, T = 1093°C(2000°F), Continuous Cycling, $N_f$ = 4,965 cy. | 67 |
| 40 | Transmission Electron Micrograph of Codep-Coated J 149 - 4 - C1 Showing Interfacial Dislocations. Test Conditions: $\Delta\varepsilon_t$ = 0.35%, T = 1093°C (2000°F), Continuous Cycling, $N_f$ = 26,330 cy. | 68 |
| 41 | Transmission Electron Micrograph of Codep-Coated K 149 - 3 - C1 Showing Dislocations in the Interface and in the Precipitates, 100,000X, Test Conditions: $\Delta\varepsilon_t$ = 0.45%, T = 1093°C(2000°F), 2 min. Compression Hold, $N_f$ = 3,693 cy. | 69 |
| 42 | Transmission Electron Micrographs of PS6MY - Coated O 151 - 1 - C2 Showing an Overall Increase in the Dislocation Density 75,000X, Test Conditions: $\Delta\varepsilon_t$ = 0.6%, Continuous Cycling, T = 1093°C(2000°F), $N_f$ = 4,653 cy. | 70 |
| 43 | Transmission Electron Micrograph of PS6MY Coated L 171 - 2 - C2 Showing Interfacial Dislocations, 42,500X Test Conditions: $\Delta\varepsilon_t$ = 0.35%, T = 1093°C(2000°F), 2 min. Compression Hold, $N_f$ = 5,149 cy. | 71 |
| 44 | Transmission Electron Micrograph of PS6MY-Coated L 171 - 2 - C2 Showing Interfacial Dislocations, 75,000X. Test Conditions: $\Delta\varepsilon_t$ = 0.35%, T = 1093°C(2000°F), 2 min. Compression Hold, $N_f$ = 5,149 cy. | 72 |
| 45 | Replica Electron Micrograph of Uncoated K 149 - 2, 15,000X Replica at 6,000 cy. Test Conditions: $\Delta\varepsilon_t$ = 0.35%, T = 1093°C(2000°F), Continuous Cycling, $N_f$ = 18,983 cy. | 73 |
| 46 | Replica Electron Micrograph of Uncoated L 151 - 3, 3,750X. Replica at 4,000 cy. Test Conditions: $\Delta\varepsilon_t$ = 0.45%, T = 1093°C(2000°F), Continuous Cycling, $N_f$ = 11,578 cy. | 74 |

| FIGURE | | PAGE |
|---|---|---|
| 47 | Replica Electron Micrograph of Uncoated L 151 - 1, 8,750X. Replica at 1,500 cy. Test Conditions: $\Delta\varepsilon_t$ = 0.6%, T = 1093°C(2000°F), Continuous Cycling, $N_f$ = 4,965 cy. | 74 |
| 48 | Replica Electron Micrograph of Uncoated L 151 - 1, 5,000X. Replica or 1,500 cy. Test Conditions: $\Delta\varepsilon_t$ = 0.6%, T = 1093°C(2000°F), Continuous Cycling, $N_f$ = 4,965 cy. | 75 |
| 49 | Replica Electron Micrograph of Codep-Coated K 149 - 3 - C1, Replica at 400 cy. 12,500X, Test Conditions: $\Delta\varepsilon_t$ = 0.45%, T = 1093°C(2000°F), 2 min. Compression Hold $N_f$ = 3,693 cy. | 76 |
| 50 | Replica Electron Micrograph of Codep-Coated L 151 - 4 - C1. Replica at 200 cy. 750X, Test Conditions: $\Delta\varepsilon_t$ = 0.6%, T = 1093°C (2000°F), 2 min. Compression Hold, $N_f$ = 1,708 cy. | 77 |
| 51 | Replica Electron Micrograph of Codep-Coated L 151 - 4 - C1. Replica at 200 cy. 250X, Test Conditions: $\Delta\varepsilon_t$ = 0.6%, T = 1093°C(2000°F), 2 min. Compression Hold $N_f$ = 1,708 cy. | 78 |

## PROJECT TEAM

| | |
|---|---|
| V. Srinivasan | Principal Investigator |
| A. W. McCormick | |
| A. K. Rai | |
| Prof. S. D. Antolovich | Consultant |

# FOREWORD

This report was prepared by the Universal Energy Systems, Inc., Dayton, Ohio under the Air Force SBIR Phase I Research Contract F33615-83-C-5119. Ft. Lt. Bryan Forston, of the Metals Behaviour Branch, MLLN/AFWAL was the Project Monitor and Dr. V. Srinivasan was the Principal Investigator. The research reported herein covered the period, October 1, 1983 to March 31, 1984.

Appreciation is expressed to Drs. R. E. Allen, T. Berry, P. K. Wright and D. Wortman, of General Electric Company, Evendale, Ohio for the gratis supply of René N4+ single crystals, heat-treatment, coatings and useful discussions. Our appreciation goes to Low Stress Grind, Inc., Cincinnati, Ohio for efficient machining; Mar-Test, Inc., Cincinnati, Ohio for LCF testing; M/S D. Wolf and J. Ziegenhagen of UDRI, R. Bowman and R. K. Payne of Georgia Tech. and A. Smith, UES for technical assistance; and Ms. T. Wilhoite and her colleagues for secretarial help.

## 1.0 INTRODUCTION

Single crystals of nickel-base superalloys have been identified as the future turbine blade material for the modern military aircrafts by the engine companies. Their choice is based on the property achievements demonstrated by screening and simulated engine tests.[1] Single crystals are the results of extensive investigation on the mechanical behavior, (especially fatigue and creep) of, and the structure-property correlations in the equiaxed and directionally solidified (DS) nickel-base superalloys. Weakness of the transverses grain boundaries in creep was recognized through creep studies. Directionally solidified (DS) and single crystal alloys with Mar-M200 composition were developed in 60's and 70's.[2,4] After the addition of Hf to DS Mar-M200, there was not much difference in the mechanical properties between single crystals and the DS version of Mar-M200. Soon it was recognized again through the mechanical property-structure correlation studies that single crystals with superior properties could be obtained by not adding the grain boundary strengtheners, Zr, B, C, and Hf. This innovation in material development has been possible because of the innovative approach to the understanding of structure-property correlations.

Turbine blades in a modern military aircraft engine operate under extreme conditions of stress, temperature and environment. No other components in such an engine operate under similar conditions. In fact, the above operating conditions of turbine blades are the direct consequences of achievements in engine thrust and fuel-efficiency. Stresses arise from centrifugal, vibratory and other mechanical and thermal origins. Combustion raises the temperature to a high value.

Oxygen in the air, salts of sodium from fuel and high temperature provide an oxidizing and hot-corrosive environment. Further, stress, temperature and environment vary in the turbine stage with time in a random fashion from the start-up (take-off) to the shut down (landing) depending on the mission and maneuver. They vary also from flight to flight. The cyclic variations of stress, temperature and enviornment may occur concurrently at different frequencies in different sequences with the interspersed intervals of constant values (hold time) of the above variable. Consequently, the high temperature fatigue, creep and oxidation-hot corrosion processes are activated in the blades.

Turbine blades in modern engines are internally air cooled. The air cooling process induces thermal gradients across the blades, and compressive stresses along the leading edges of the blades. Experience has been that cracks appear at the leading edges of blades in the accelerated engine tests and in service. These cracks have their origin in thermal-mechanical fatigue processes.

We may therefore conclude that the thermal-mechanical fatigue with attended creep damage, and oxidation-hot corrosion are the life limiting processes in turbine blades.

The above processes are microstructure-sensitive. They are therefore to be studied in every turbine blade alloy, and more so in each new alloy.

The blade alloys are inherently poor in their oxidation-hot corrosion resistance. Therefore, they have protective coatings. The blade alloys and their coating differ considerably in their physical and mechanical properties. Consequently the mechanical behavior of the

blade-coating composite is most likely to be different from that of the substrate, and could have adverse consequences. There are two different types of coatings. They are the conventional aluminide coating and the overlay coating with improved temperature capability.[5] These coatings in turn affect differently the mechanical behavior of the coated blade.

With the increasing cost of manufacturing and replacement of high performance blades and vanes, it becomes economically necessary to retire components only at the end of their full service life without impairing the effective performance of the engine. This is possible only with a reliable life prediction technology. Innovative approach is required for the development of life prediction technology because of the difficulties in extending the laboratory specimens' results to describe the actual service behavior of components. A way to overcome these difficulties is to understand the micromechanisms of damage accumulation and apply the equivalent damage concept. The accomplished Phase I research and the proposed Phase II research are innovative in the sense that they try to improve our understanding of the basic life limiting process in the new single crystal alloys for better description of the synergism in service condition, and to contribute to the development of stronger high temperature alloys through the structure-property relations. It is only through the understanding of the structure-property relations that the development of stronger higher temperature alloys has been posible.

The Phase I research was an exploratory effort to demonstrate the application of various techniques to understand the crack nucleation and propagation process that determines the fatigue life at elevated temperatures. A comprehensive description of the research accomplished

and the results obtained are given along with the estimate of technical feasibility of the experimental approach.

## 2.0 TECHNICAL OBJECTIVES

The technical objective of Phase I was to obtain some preliminary information on the life and on the nature of damage accumulation during high temperature low cycle fatigue in single crystal nickel-base superalloy, René N4+. This objective was examined on crystals for the orientation of practical importance with and without high temperature protective coatings. Further, it included development and standardization of procedures for preparation of thin foil and replica for TEM examination.

Phase I tried to answer a few questions, such as:

- What is the relation between strain-range and number of cycles to failure?
- What is the nature of damage in the single crystal nickel-base superalloy that limits the life in isothermal high temperature low cycle fatigue?
- Is there more than one damage process occurring simultaneously? (for example, coarsening of gamma prime and environmental interaction?)
- How does the high temperature coating affect the isothermal high temperature low cycle fatigue process of the substrate?
- What is the role of slip bands, twin boundaries, etc., in crack initiation in specimens with and without coatings?

## 3.0 EXPERIMENTAL ALLOY AND METHOD

### 3.1 EXPERIMENTAL ALLOY

Cast René N4+ in single crystal form was chosen for this research. It is a nickel-base superalloy selected for engine application in the 1980s. Its composition is derived from that of René N4 which is given in Table I. Cast slabs with the growth orientation close to [001] were received gratis from Dr. R. E. Allen, Aircraft Engine Business Group, Evendale, Ohio. These slabs had been checked for their soundness and released for this study. Inspection of these slabs for the growth directions had revealed acceptable deivations as given in Table II. Four rectangular blanks were machined from each slab, and were given solution heat treatment. Low cycle fatigue test samples were machined with the final low-stress grinding from the above solution-heat treated blanks according to the dimensions shown in Figure 1. Machined samples were divided into three batches. A set of eight specimens received Codep coating and the second set of eight samples were given plasma-spray PS6MY coating. Bare and coated samples went through diffusion heat treatment and the final ageing. Heat treatments and coatings were done at the General Electric facility, Evendale, Ohio. The final low-stress machining of coated samples resulted in smooth surface finish. The thickness of Codep and PS6MY coatings were about 2 to 2.5 and 6 to 8 mils respectively.

### 3.2 HIGH TEMPERATURE LOW CYCLE FATIGUE TEST

High temperature low cycle fatigue tests were performed at Mar-Test, Inc., Cincinnati, Ohio. Electro-hydraulic servo controlled test machines were used. Load cell and extensometer were calibrated.

The test specimen was mounted into the grips forming part of the load-train. The specimen was surrounded by a R.F. coil, and was heated during the test by a Lepel induction generator. While mounting the sample, care was taken not to cause any surface damage or buckling. The axial extensometer was mounted onto the specimen between the gage marks. By elastic deformation, the Young modulus at RT and at the test temperature was measured. With an almost zero load, the sample was heated. As the sample expanded, the grips were automatically moved by load control to avoid buckling. Once the sample reached the test temperature of 1093°C (2000°F), the axial strain control was activated, and the strain limits in tension and compression were set. Periodically hysteresis loops were traced. All tests were fully reversed with the strain ratio $R = -1$ and $A = \infty$. The final failure was reckoned either with the actual sample break-up or with a 60% fall in the peak load. Those samples which did not break at the test temperature, were broken later at room temperature. A few tests were stopped short of failure, and were referred to as the Run-out tests.

To take the surface replica during a test, the specimen load was reduced to a small (10%) tensile value, and the machine was switched to the load control. The heating was shut down. As the specimen cooled down to the room temperature, the load control kept the load at a low tensile value. After ensuring the access to the specimen surface, a replicating tape moistened with acetone was pressed around the gage diameter with the finger pressure and left to acquire the surface features. The dried replicating tape was gently removed, and preserved for microscopic observations.

Two types of LCF tests were performed on the bare and the coated samples. Continuous cycling tests were conducted at 20 cpm. Hold-time tests with 2 min. hold in compression were chosen to simulate the condition at the leading edge of a blade in service. The wave form for continuous cycling test was triangular, and over this wave form superimposed was a 2 min. compression hold,(Figure 2). The test Matrix is shown in Table III. All samples failed within the gage length.

## 3.3 MICROSTRUCTURAL EXAMINATION

### 3.3.1 Fractography

Fracture surfaces were examined to identify the crack initiation sites. They were carefully cut from the broken test pieces using an Isomet saw and cleaned ultrasonically. They were examined in the JEOL and Cambridge scanning electron microscopes with EDAX facility.

### 3.3.2 Examination of Longitudinal Sections

Longitudinal sections were cut using an Isomet saw. They were mounted and polished metallographically. After the final ultrosonic cleaning, they were etched with Rifess etch. The composition of the etchant is:

6 parts of Water with 4 parts of Modified Tucker's etchant.

The modified Tucker's etchant is as follows:

| | |
|---|---|
| Water ($H_2O$) | 25 ml |
| Hydrochloric Acid (HCl) | 45 ml |
| Nitric Acid ($HNO_3$) | 15 ml |
| Hydrofluoric Acid (HF) | 15 ml |
| Cupric Chloride | 10 gr |

The etchant's action was fast, and etching was completed in a few seconds. Several transverse sections were examined in the JEOL scanning microscope which has the EDAX attachment. To avoid the specimen charging inside the microscope, a thin layer of gold coating was given.

3.3.3 Transmission Electron Microscopy

Thin foils were prepared from the as heat-treated René N4+ as well as from the tested samples. Slices of 15 to 20 mil thickness were cut with a low speed Isomet saw. A single jet electro-polishing unit was employed to get thin foils from the slices. Initially several electrolytes and polishing condtions were used. The following two were chosen for the rest of Phase I research.[4,6]

(1) Methanol 83%
Sulfuric Acid 7.5%
Nitric Acid 3.0%
Hydrofluoric Acid 2.0%
Lactic Acid 4.5%
Room Temperature
Voltage = 10V [4]

(2) Perchloric Acid 10%
Acetic Acid 90%
Voltage 65V
Temperature 18°C

Success and reproducibility were better with the latter electrolyte and the polishing condition.

Replicas were first shadowed with gold, and later carbon was deposited uniformly. Pieces were cut and dropped in a watch glass containing acetone. When the plastic tape got dissolved, the carbon replica floated on the surface. Carefully the floating replica was picked up with copper grids.

Hitachi H-600 scanning and transmission electron microscope was used to examine the thin foils and the replicas at 100KV. Bright field, dark field and diffraction techniques were employed. Different g vectors were chosen to study the dislocations.

## 4.0 RESULTS AND DISCUSSION

### 4.1 MECHANICAL TEST RESULTS

Low cycle fatigue life increase with the decreasing total strain range in all the three cases of bare and coated single crystals under both the continous cycling and hold time conditions. The relationships between the total strain range and number of cycles to failure are given for various test condtions in Figures 3-5. A comparison of the above relationships is made in Figure 6, and Table V gives the test data.

The total strain range follows the relation

$$\Delta\varepsilon_t = \text{Const. } N_f^{\alpha}$$

in determining the number of cycles to failure ($\alpha \simeq 0.4$ and 0.6 for continuous and hold-time tests).

$N_i$ in Table IV represents the number of cycles to initiate cracks and was identified during a test by the drop in the peak load. This value seems to be a gross over estimate as the surface replication indicated much earlier crack nucleation ($\Delta\varepsilon_t$ vs $t_f$ is given in Figure 7).

Hysteresis loops were traced periodically during the tests. Figures 8 and 9 represent the trends observed in all continuous cycling and hold time tests. The mean stress in the hold time tests appears to become more positive as the test progressed.

## 4.2 METALLOGRAPHY RESULTS

### 4.2.1 Scanning Electron Microscopy

Three types of microstructural examination were carried out using the scanning electron microscope and the energy dispersive analysis by x rays. The fracture surfaces of the failed samples were studied. In almost all the cases the high temperature fracture surface was covered with oxides. There were a few areas where the oxide scales had fallen from the fracture surfaces. In those samples which were pulled at room temperature after high temperature low cycle fatigue tests to complete the fracture process, carbide cracks were seen in the RT fracture zones. The RT fracture surface did not have oxides. The typical fracture surfaces are shown in Figures 10-19. Figure 10 brings out the features of high temperature LCF fracture in a sample (L 151 - 1) which failed after 4965 cycles (248.2 min.) under continuous cycling at a strain range of $\Delta\varepsilon_t$ = 0.6%. Several cracks had nucleated and traveled inward. The high temperature fracture areas (Figures 10b and 11a) are covered with oxides. The oxides in Figure 11a have a hazy appearance resembling the texture of cotton candy. Room temperature fracture has a different appearance (Figure 11b). The effect of hold time 2 min. in compression is seen in Figure 12a on the fracture under the same strain range of $\Delta\varepsilon_t$ = 0.6%. Numerous surface cracks had nucleated in this sample

(E 151 - 2) which failed in 1755 cycles (3597.8 min.). Figures 12b, 13a and 13b elaborate the features seen near a few nucleation sites. Fine oxide particles are seen on the high temperature fracture areas. The fracture surfaces of the Codep coated sample (L 151 - 4 - C1) are shown in Figures 14a and 14b. The LCF life of this sample at $\Delta\varepsilon_t$ = 0.6% is 1708 cycles (3501.4 min.) under 2 min. hold in compression. The above sample differs from E 151 - 2 only in the surface conditions; while L 151 - 4 - C1 had Codep coating, E 151 - 2 was bare. Oxide particles are seen on the fracture surface including the cross section of the fractured coating (Figure 14 a). The oxides away from the coating are angular (Figure 14b). The room temperature fracture regions of the sample, L 151 - 4 - C1, show microvoid coalescence (Figure 15b) in the substrate, decohesion of Codep coating and the brittle failure of coating (Figure 15a). Casting defects such as micro pores are seen on the room temperature fracture surface of this sample (Figure 15b). In the sample (K 149 - 3 - C1) tested at $\Delta\varepsilon_t$ = 0.45% with a 2 min. compression hold, the fracture surface was characterized by flat and slant fracture regions and wedges (Figure 16a). A typical effect of hold time was to cause numerous circumferential cracks along the gage length, and one such crack is shown in Figure 16b. This crack is deep and connected with the fracture surface. This sample survived 3693 cycles (7570.7 min.). The oxide morphology in this case, (Figures 17a and 17b) differs from that observed in the sample L 151 - 4 - C1, (Figure 14). The test condtions of the above samples were the same except for the strain range. In this case (K 149 - 3 - C1) oxides are more rounded and look like pebbles. When the strain range was reduced to 0.35%, the outer region of the coating fracture surface remained free from oxides, (Figure 18a; Sample

J 149 - 4 - C1), under continuous cycling. The oxides covering the substrate fracture surface appear to be relatively finer (Figure 18b). The above specimen failed in 26330 cycles (1316.5 min.). When the above strain range, $\Delta\varepsilon_t$ = 0.35% was combined with a 2 min. compression hold, the fracture surface morphology of Codep coating and the substrate changes as shown in Figures 19a and 19b. The sample here is E 151 - 3 - C1 with a life of 5311 cycles (10,888.2 min). There are cracks at the coating-substrate interface suggesting decohesion (Figure 19a) and the oxides are contiguous (Figure 19b).

Transverse cracks and cracks below the fracture surface were seen in the polished and etched longitudiual sections under scanning electron microscope. Their numbers and geometry depended on the test condtions. Most of the cracks had reacted zones along their lengths indicated by distinct gray color. Figure 20a shows two transverse cracks originated from the surface. (The test specimen: K 149 - 2 and the test condtions: $\Delta\varepsilon_t$ = 0.35% and continuous cycling). No other transverse cracks or subfracture surface cracks were seen in this sample. Several subfracture surface cracks connected with the fracture face were seen when the strain range was high, $\Delta\varepsilon_t$ = 0.6%, (Figure 21; Sample L 151 - 1, continuous cycling). Oxidation had occurred in general along the sides of the bare specimen during the high temperature test. In the case of sample L 151 - 1 ( $\Delta\varepsilon_t$ = 0.6%; continuous cycling; uncoated) oxidized subsurface region stands out (Figure 22a). The thickness of this reacted zone can be calculated from the diffusion coefficient of oxygen at 1093 °C and the time of high temperature exposure. EDAX (Energy Dispersive Analysis by X rays) spectra were taken from the interior as

well as from the oxidized (light gray) region. They are shown respectively in Figures 22b and 22c. Oxidation seems to deplete chromium and titanium in this region. There are inclusions such as those shown in Figure 23a. Inclusion of this kind, according to the EDAX spectrum, Figure 23b is rich in Ta and Ti and has relatively low Ni and Cr suggesting Mc-type carbides.

Several transverse cracks have nucleated during the LCF test with $\Delta\varepsilon_t$= 0.6% under continuous cycling (L 151 - 1). Figure 24a shows two such cracks originated at points close to each other on the surface. They are diverging, and one of them is dominant. A short crack appears to have nucleated at the surface in an oxidized inclusion (Figure 24b). Secondary cracks below the fracture surface of the sample E 151 - 2 are shown in Figures 25a and 25b. Some of them are connected with the fracture surface. Numerous transverse cracks with varying lengths are seen in the longitudinal sections of the sample E 151 - 2 (Figures 26a and 26b). The above sample was fatigued at$\Delta\varepsilon_t$ = 0.6% with a 2 min. hold in compression.

Transverse cracks behaved differently in the aluminide (Codep) coated René N4+, and an example is given in Figure 27a (Sample J 149 - 4 - C1). A number of transverse cracks are initiated on the coating surface, and most of them stop at the inner diffusion zone. EDAX spectra taken from the outer region, the diffusion zone and the substrate are shown in Fiugres 28a , 28b and 28c respectively. In the above sample, secondary cracks below the fracture surface are not many but those present are long and surface-connected as shown in Figures 29a and 29b. The above the Codep-coated sample J 149 - 4 - C1 was subjected

to a strain range of $\Delta\varepsilon_t$ = 0.35% under continuous cycling. Significant changes in the density and the length of the transverse cracks and in the substrate microstructure occur in the Codep-coated René N4+ when a 2 min. hold time was introduced. These changes are shown in Figures 30 and 31. The sample E 151 - 3 - C1 underwent the LCF test with $\Delta\varepsilon_t$ = 0.35% and a 2 min. hold time in compression. Considerable rumpling and spalling of the coating along with longer transverse cracks are seen in Figures 30a and 31a. Needle phases are seen in the substrate close to the diffusion zone. A long transverse crack with branches was present below the fracture surface connecting the side and the fracture face (Figure 31a). The overlay coating has different effect on the transverse cracks. Figure 32 describes the observations made on the sample L 171 - 1 - C2. This sample with the PS6MY coating was tested at $\Delta\varepsilon_t$ = 0.35% under continuous cycling. Only one or two short transverse cracks lying within the coating were seen. However, when a 2 min. hold time in compression was introduced in the test with $\Delta\varepsilon_t$ = 0.35%, not only several transverse cracks, but a few long ones were observed as shown in Figures 33a, 33b, and 34a. Here the sample is L 171 - 2 - C2. Oxidation along the cracks edges is not as distinct as it is observed in the case of bare and Codep-coated René N4+.

The gamma prime precipitates, $\gamma'$, coarsened during the LCF test. The extent of their coarsening and linking are dependent on the test conditions. A few examples are shown in Figures 20b, 27b, 31b, 32b, and 34b.

### 4.2.2 Transmission Electron Microscopy

The transmission electron diffraction pattern of heat-treated René N4+ is shown in Figure 35a. Both the matrix and the superlattice spots are present. The symmetry of the diffraction pattern suggests that the cube faces of the gamma prime, $\gamma'$ precipitates are parallel to the {100} planes of the matrix.

Figures 35b and 35c are the bright field and the dark field images respectively of a typical region in the heat-treated alloy. The dark filed image was obtained with the diffraction spot, 200, there are no interfacial dislocations visible at this magnification. At a higher magnification a few dislocations in the matrix and in the precipitates are seen (Figures 36 and 37). These bright field images are taken from the same area in the thin film with different $\vec{g}$ vectors. A few interfacial dislocations suggest good coherency between the matrix and the precipitates. A preliminary analysis suggests that the dislocations are of edge type with Burger's vector $\frac{a}{2}$ <110>.

The transmission electron micrographs of samples (K 149 - 2 and L 151 - 1) tested under continuous cycling with strain ranges 0.35% and 0.60% respectively are shown in Figures 38 and 39. The precipitates are relatively free from dislocations, while the interfacial dislocation density has increased. The precipitates after the test become more rounded, and most of them are still disconnected. However, the change in the precipitate shape, the joining of precipitates and a significant increase in the interfacial dislocation density are noticable in the case of Codep-coated sample (J 149 - 4 - C1) tested in continuous cycling with $\Delta\varepsilon_t = 0.35\%$ (Figures 40a and 40b.) Most of the gamma prime precipitates

are almost free from dislocations. The introduction of a 2 minute compression hold in a LCF test with $\Delta\varepsilon_t$ = 0.45% brings about dislocation activity in the gamma prime precipitates (Figure 41; Sample K 149 - 3 - C1). Increase in the dislocation density in the precipitates and in the matrix is evident in the PS6MY-coated sample 0151 - 1 - C2 which was tested at a high strain range of 0.6% under continuous cycling condition. Even though the test involved hold time, not many dislocations are seen in the precipitates and in the matrix in the PS6MY-coated sample L 171 - 2 - C2, possibly because of low strain range, $\Delta\varepsilon_t$ = 0.35%, (Figures 43 and 44). The elongation of the precipitates is obvious in this sample.

The electron micrographs of the surface replicas are shwon in Figures 45 to 51. Many surface-initiated circumferential cracks are seen in them. They are almost normal to the stress axis. The examinations of the replicas in TEM suggest that the number of surface cracks increases with increasing strain range and that for a given strain range, the hold time causes more surface and internal cracks.

## 4.3 DISCUSSION

Low cycle fatigue life is determined in principle by the crack nucleation and the propagation processes. These processes are not always equally important, and the dominant one determines the specimen's life. Normally the crack nucleation occurs at the weak links in the material. Cracks nucleate depending on the test conditions, on the free surface or in the interior, wherever the weak links are present and the deformation

conditions are favorable. At high temperatures, the time dependent processes such as the surface oxidation and creep affect the nucleation and the propagation processes.

Multiple crack nucleation sites are discernible in the present work on the fracture surfaces of René N4+. Almost all of them are on the free surface. The transverse cracks observed on the longitudinal sections of the uncoated and the coated samples have geometries which suggest the free surface as their origin. The transverse cracks away from the fracture location are not deep. Many secondary cracks are observed below the fracture surfaces, and they are connected to the free surface as indicated by the oxide envelope around them. It therefore looks as though the fracture location was determined in the gage length by the density of cracks nucleated in the early fatigue life. The nucleation and the early propagation of cracks on the fracture surfaces have occurred in State II mode. Subsequently the crack growth mode has changed to Stage I. However, the other transverse cracks on the longitudinal sections did not exhibit, at least on the sections examined, such a mode change.

The cuboidal gamma prime, $\gamma'$ precipitates become rounded in many samples. The increase in the interfacial dislocations indicate significant coarsening of the precipitates.[6] Extensive coarsening and the link-up of the precipitates, $\gamma'$ are noticed particularly under the compression hold condition at the high strain range. The mean (positive) tensile stress is believed to be responsible for this behavior.

Many crack nucleation sites have been reported in directionally cast single crystals.[7-9] They have been mostly observed after the

tension-tension LCF/HCF tests with and without the tensile hold times. When the grain boundaries are absent, the casting micropores and the carbides become the preferred crack nucleation sites. Crack nucleation occurs on the free surface and in the interior. At low temperatures and high frequencies the carbides provide the nucleation sites. The high strength and the low ductility of the alloy at low temperatures promote carbide cracking. The fatigue cracks have also been observed to nucleate at the precracked carbides.[9] These carbides are either on the free surface or in the interior. A good correlation exists between the carbide size and the LCF life at low temperatures.[10] Further, planar slip at these temperatures results in Stage I crack nucleation and propagation.[8] As the test temperature is increased, changes occur in the strength, the ductility, the deformation mode and the oxidation resistance of the alloy. Planar slip is no longer the dominant deformation mode, and the slip dispersal becomes possible. Consequently the carbide cracking does not occur, and the casting micropores become the favorable crack nucleation spots. The secondary role of carbides in the high temperature crack nucleation process is brought out by the obsence of any systematic variation between the carbide size and the LCF life.[9] Crack nucleation and crack propagation occur in State II, as observed in René N4+. When the crack length reaches a certain length, the deformation rates at the crack tip changes the propagation mode to State I.[8]

Surface crack nucleation observed in Phase I research appears to be characteristic of René N4+ within the test conditions examined. It is speculated that the cracks are nucleated in the bare samples at the

casting micropores on the surface, since no cracks are found associated with the interior micropores. In the case of coated samples the nature of surface defects that localize the crack nucleation process is not clear. However, once nucleated on the surface of the coatings, a few cracks find their way deep into the substrate to cause final failure.

Early nucleation of surface crack is indicated by the limited replica work. Therefore, the importance of crack growth has to be established. The oxidation of exposed fracture surface may affect the crack growth process by introducing the closure phenomenon.

The present result indicates a good correlations between the total strain range and the cycles to failure. The damaging processes appear to be the gamma prime, $\gamma'$ coarsening, the precipitates, $\gamma'$ link-up and the oxidation processes. Further research in Phase II micromechanical models can be developed based on the microstructural changes and the oxidation processes.[12-14]

## 5.0 CONCLUSIONS

Evidences are that cracks are nucleated in René N4+ under the test condtions considered here early in the LCF life. Multiple cracks are initiated on the surfaces of uncoated and coated samples. The casting micropores on the surface of the bare samples are believed to be the preferred sites of crack initiation. The nature of surface defects at which cracks nucleate in the case of Codep- and PS6MY-coated samples is not clear. The surface-nucleated cracks propagate inward initially in Stage II mode. Later the mode of propagation changes to Stage I. The final fracture is caused by multiple cracks nucleated on the fracture surface. The fracture location in the gage length appears to coincide

with the section where the density of cracks is more. The precipitate coarsening and joining occurs. High strain range and compression hold time cause an increase in the number of surface-nucleated cracks, and promote coarsening and elongation of the precipitates. Oxidation of the exposed fracture surface occurs during the test, and the oxides cover the fracture surface. Coatings do not affect significantly the isothermal LCF lives of René N4+. The isothermal LCF lives of René N4+ can be adequately described by empirical relations similar to that of Coffin-Manson.

The Phase I research brings out the importance of the precipitate coarsening, the role of casting micropores, the mean tensile stress, the oxidation and the crack propagation in the LCF behaviour of René N4+. Their relationship need be understood in other test conditions to develop a life prediction method with greater applicability. Crack growth studies and a fracture mechanic approach to describe the propagation of multiple short cracks may be required to describe the crack growth in René N4+ under the LCF condition. The oxides particles on the fracture surface may cause closure effects during low cycle fatigue.

## 6.0 ESTIMATE OF TECHNICAL FEASIBILITY

The objectives of Phase I and Phase II research are to understand the damage processes that occur in René N4+ single crystals under LCF conditions and to develop a life prediction methodology for the laboratory specimens. The Phase I results have indicated the weak links in René N4+ where the cracks are nucleated under the isothermal LCF conditions and the role of mean stress and oxidation. The LCF testing and the metallographic techniques such as TEM, SEM, replica, longitudinal

sectioning and fractography have contributed to the understanding of crack nucleation process, load-strain effects, the microstructural changes and the oxidation effects in the uncoated and coated samples. The success of Phase I research strongly suggests the technical feasibility of the approach. In Phase II complex situations will be studied where the effects of coating will be significant. The results of Phase II are expected to improve our understanding of crack nucleation and propagation processes in René N4+ in terms of micro- and macro-mechanisms and to lead to a life prediction methodology valid under the complex conditions of fatigue, creep and thermal oxidation.

The U.S. Air Force and the Engine Companies could use the Phase II results as base line informations, and apply them through the concept of equivalent damage to estimate the blade lives.

## REFERENCES


1. M. Gell, D. N. Duhl and A. F. Giamei in "Superalloys 1980," eds. J. K. Tien, S. T. Wlodek, H. Morrow III, M. Gell and G. Maurer. ASM, Cleveland, OH (1981), 205

2. G. R. Leverant, B. H. Kear and J. M. Oblak, Met. Trans. 4 (1973), 355

3. B. H. Kear, S. M. Copley and F. L. VerSnyder, Trans. JIM 9 (1968) Supplement, 672

4. G. R. Leverant and B. H. Kear, Met. Trans. 1 (1970), 491

5. C. T. Sims and W. C. Hagel, "Superalloys," John Wiley (1972).

6. A. Lasalmonie and J. L. Strudel, Phil. Mag. 32 (1975), 937

7. D. J. Duquette and M. Gell, Met. Trans. 3 (1972), 1899

8. M. Gell and G. R. Leverant, in "Fatigue at Elevated Temperatures," ASTM-STP (1973), 37

REFERENCES (con't)


9. G. R. Leverant and M. Gell, Trans. AIME, 245 (1969), 1167

10. M. Gell and G. R. Leverant, Trans. AIME 242 (1968), 1869

11. S. D. Antolovich, AFOSR-TR-83-0827

12. S. D. Antolovich, S. Liu and R. Baur, Met. Trans. 12A (1981), 473

13. J. Reuchet and L. Remy, Met. Trans. 14A (1983) 141

14. S. D. Antolovich, S. Liu and R. Baur, in "Superalloys 1980," ed. J. K. Tieu, S. T. Wlodek, H. Morvow III, M. Gell and G. Maurer, ASM, Cleveland, OH (1981), 605


0088j

TABLE I

NOMINAL CHEMICAL COMPOSITION OF René N4, Wt. %

| Ni | Cr | Co | Mo | W | Ta | cb | Al | Ti |
|---|---|---|---|---|---|---|---|---|
| Bal | 9.25 | 7.7 | 1.5 | 6.0 | 4.0 | 0.5 | 3.7 | 4.2 |

TABLE II

ORIENTATION OF CAST DIRECTION WITH RESPECT TO [001]

| SLAB I.D. | PRIMARY ORIENTATION FROM [001] |
|---|---|
| O 151 | 4.5° |
| E 151 | 4.0° |
| L 151 | 10.5° |
| J 149 | 7.5° |
| K 149 | 10.5° |
| L 171 | 9.0° |

TABLE III

TEST MATRIX
Fully Reversed, A = (R = -1)
Test Temperature 1093°C (2000°F)

| Strain Range, % | Bare | | Codep Coated | | PS6MY Coated | |
|---|---|---|---|---|---|---|
| | Cont.* | Hold** | Cont.* | Hold** | Cont.* | Hold** |
| 0.35 | x | x | x | x | x | x |
| | RP(6000) | - | - | - | RP(2000) | - |
| 0.45 | x | x | x | x | x | x |
| | RP(4000) | RP(400) | - | RP(400) | - | - |
| 0.60 | x | x | x | x | x | x |
| | RP(1500) | RP(200) | - | RP(200) | - | RP(200) |

* Continuous Cycling at 20cpm; Triangular Wave Form

** Two min. hold in compression

RP(X), Plastic replica taken after x cycles

# TABLE IV

ALPHA = 9.7 x 10**-6/DEG. F
SPECIMEN DESIGN:

LCF DATA SUMMARY FOR RENE N-4
AXIAL STRAIN MEASUREMENT AND CONTROL
(Continuous cycling tests and tests
with hold period in tension and compression)

ENGINEER: SRI
P.O. NO.: 738-5
JOB NO.: 083-901

| SPECIMEN NUMBER | MTS MACH. NO. | R.T. DIA. IN. | TEST TEMP. DEG. F | AREA AT TEST TEMP. SQ. IN. | E AT R.T. 10**6 PSI | E AT TEMP. 10**6 PSI | E AT TEMP. MEASURED IN SELECTED CYCLE 10**6 PSI | CYCLE | AT START: STRAIN RANGE % | AT START: STRAIN RATIO *A* | AT START: PSEUDO STRESS RANGE KSI | AT N#/2: STRESS RANGE KSI | AT N#/2: MAX. STRESS KSI | AT N#/2: MIN. STRESS KSI | AT N#/2: STRESS RANGE KSI | AT N#/2: MAX. STRESS KSI | AT N#/2: MIN. STRESS KSI | AT N#/2: ELASTIC STRAIN RANGE % | AT N#/2: PLASTIC STRAIN RANGE CALC. % | AT N#/2: PLASTIC STRAIN RANGE MEAS. % | N# CYCLES | N# CYCLES | N# MINUTES | REMARKS |
|---|---|---|---|---|---|---|---|---|---|---|---|---|---|---|---|---|---|---|---|---|---|---|---|---|
| WAVEFORM = TRIANGULAR 20 CPM | | | | | | | | | | | | | | | | | | | | | | | | |
| K149-2 | 27 | .2003 | 2000 | .0327 | 19.5 | 10.1 | 10.8 | 5750 | .35 | INFINITY | 35.4 | 34.3 | 16.7 | -17.6 | 34.6 | 18.3 | -16.3 | .34 | .01 | .03 | 16643 | 18983 | 949.2 | B. |
| L171-1 | 27 | .1988 | 2000 | .0351 | 20.3 | 12.1 | 11.5 | 2727 | .60 | INFINITY | 72.6 | 64.3 | 31.7 | -32.6 | 60.2 | 30.1 | -30.1 | .50 | .10 | .11 | 4351 | 4965 | 248.3 | A.B. |
| L151-3 | 27 | .1999 | 2000 | .0326 | 19.4 | 10.5 | 10.4 | 4496 | .45 | INFINITY | 47.3 | 41. | 19.0 | -22.1 | 39.7 | 21.2 | -18.5 | .38 | .07 | .05 | 9752 | 11578 | 578.9 | A.B. |
| J149-4-C1 | 34 | .2001 | 2000 | .0325 | 19.9 | 10.3 | 10.1 | 5310 | .35 | INFINITY | 36.1 | 35.5 | 17.9 | -17.7 | 32.4 | 18.9 | -13.5 | .31 | .04 | .05 | 25050 | 26330 | 13.5.5 | A.B. |
| K149-1-C1 | 34 | .2014 | 2000 | .0331 | 19.3 | 9.9 | 9.5 | 2264 | .45 | INFINITY | 44.6 | 41.5 | 20.4 | -21.1 | 33.9 | 16.8 | -17.1 | .34 | .11 | .14 | 9190 | 9880 | 494.0 | A.B. |
| L171-1-C2 | 20 | .2007 | 2000 | .0352 | 20.5 | 9.5 | 9.2 | 2149 | .35 | INFINITY | 33.3 | 32. | 16.2 | -15.8 | 26.9 | 14.1 | -12.8 | .28 | .07 | .09 | 14292 | 16072 | 803.6 | A.B. |
| *L171-1-C2 REPLICATED AT 2000 CYC. | | | | | | | | | | | | | | | | | | | | | | | | |
| E151-3-C2 | 20 | .2080 | 2000 | .0353 | 20.8 | 9.0 | 8.9 | 1889 | .45 | INFINITY | 40.5 | 38. | 17.8 | -16.3 | 33.9 | 15.5 | -17.3 | .37 | .09 | .13 | 9681 | 10701 | 536.1 | A.B. |
| E151-1-C2 | 20 | .2078 | 2000 | .0357 | 19.8 | 8.6 | 9.1 | 446 | .60 | INFINITY | 52.8 | 46. | 24.1 | -21.9 | 36.0 | 19.1 | -17.0 | .41 | .19 | .23 | 4037 | 4659 | 232.6 | A.B. |
| *E151-1-C2 REPLICATED AT 500 CYC. | | | | | | | | | | | | | | | | | | | | | | | | |
| WAVEFORM = TRAPEZOIDAL: HOLD PERIOD IN TENSION FOR 2.00 MIN. WITH 0.05 MIN. RAMP TIME. | | | | | | | | | | | | | | | | | | | | | | | | |
| E151-4 | 27 | .1991 | 2000 | .0322 | 19.5 | 11.1 | 11.2 | 2335 | .45 | INFINITY | 50.0 | 46.6 | 20.0 | -26.6 | 42.4 | 13.5 | -28.9 | .38 | .07 | | 0 | 4218 | 8646.9 | R. |
| (RELAXED VALUES) | | | | | | | | | | | | 42.4 | 15.8 | | 36.2 | 7.3 | | .33 | .12 | .13 | | | | |
| WAVEFORM = TRAPEZOIDAL: HOLD PERIOD IN COMPRESSION FOR 2.00 MIN. WITH 0.05 MIN. RAMP TIME. | | | | | | | | | | | | | | | | | | | | | | | | |
| 0151-2-C2 | 20 | .2005 | 2000 | .0328 | 21.7 | 10.3 | 10.7 | 736 | .60 | INFINITY | 61.8 | 53.8 | 30.1 | -23.7 | 54.2 | 35.7 | -18.5 | .53 | .07 | | 1158 | 1911 | 3917.6 | A.B. |
| (RELAXED VALUES) | | | | | | | | | | | | 47.7 | | -17.6 | 47.6 | | -11.9 | .46 | .14 | .20 | | | | |
| E151-2 | 27 | .1984 | 2000 | .0321 | 20.0 | 11.0 | 11.4 | 859 | .60 | INFINITY | 66.0 | 57.8 | 33.1 | -23.9 | 56.5 | 38.3 | -18.2 | .51 | .09 | | 1317 | 1755 | 3597.8 | B. |
| (RELAXED VALUES) | | | | | | | | | | | | 52.2 | | -19.1 | 50.8 | | -12.5 | .46 | .14 | .15 | | | | |
| E151-3-C1 | 9 | .2017 | 2000 | .0332 | 20.4 | 10.5 | 9.9 | 2791 | .35 | INFINITY | 36.8 | 34.1 | 20.1 | -16.0 | 31.9 | 19.6 | -12.1 | .30 | .05 | | 4156 | 5311 | 10888.2 | A.B. |
| (RELAXED VALUES) | | | | | | | | | | | | 34.4 | | -14.3 | 27.3 | | -7.5 | .26 | .09 | .09 | | | | |
| J149-1 | 34 | .1995 | 2000 | .0323 | 18.9 | 10.7 | 10.4 | 4171 | .35 | INFINITY | 37.5 | 37.5 | 20.7 | -16.8 | 34.0 | 23.9 | -10.1 | .32 | .03 | | 0 | 4171 | 8550.6 | R. |
| (RELAXED VALUES) | | | | | | | | | | | | 36.6 | | -15.9 | 30.2 | | -6.3 | .28 | .07 | .07 | | | | |
| K149-3-C1 | 9 | .1996 | 2000 | .0325 | 19.8 | 10.2 | 10.1 | 1600 | .45 | INFINITY | 45.9 | 41.4 | 23.9 | -17.5 | 37.5 | 23.3 | -14.2 | .37 | .08 | | 2320 | 3693 | 7570.7 | A.B. |
| (RELAXED VALUES) | | | | | | | | | | | | 37.7 | | -13.1 | 32.2 | | -8.9 | .32 | .13 | .16 | | | | |
| L151-4-LC. | 34 | .2013 | 2000 | .0330 | 19.4 | 9.8 | 9.6 | 901 | .60 | INFINITY | 58.8 | 50.4 | 30.1 | -20.3 | 45.1 | 30.4 | -14.7 | .46 | .14 | | 1326 | 1708 | 3501.4 | A.B. |
| (RELAXED VALUES) | | | | | | | | | | | | 44.5 | | -14.4 | 38.9 | | -8.5 | .40 | .20 | .22 | | | | |
| K149-4 | 34 | .2005 | 2000 | .0329 | 18.6 | 9.9 | 10.4 | 692 | .45 | -1.0 | 44.6 | 43.1 | 21.1 | -22.0 | 40.2 | 28.5 | -11.7 | .41 | .04 | | 2193 | 2733 | 5602.7 | A.B. |
| (RELAXED VALUES) | | | | | | | | | | | | 48.5 | | -19.4 | 34.8 | | -6.3 | .35 | .10 | .12 | | | | |
| 0151-4-C2 | 22 | .2082 | 2000 | .0350 | 19.6 | 9.4 | 9.0 | 2600 | .45 | INFINITY | 42.3 | 41.0 | 24.3 | -16.7 | 35.8 | 22.6 | -13.2 | .38 | .07 | | 2752 | 3479 | 7132.0 | A.B. |
| (RELAXED VALUES) | | | | | | | | | | | | 37.1 | | -12.9 | 31.1 | | -8.5 | .33 | .12 | .14 | | | | |
| L171-2-C2 | 23 | .2083 | 2000 | .0353 | 20.6 | 10.0 | 10.4 | 2819 | .35 | INFINITY | 35.0 | 34.7 | 19.8 | -14.9 | 34.0 | 22.3 | -11.7 | .34 | .01 | | 4049 | 5149 | 10555.4 | A.B. |
| (RELAXED VALUES) | | | | | | | | | | | | 33.2 | | -13.5 | 30.6 | | -8.3 | .31 | .04 | .07 | | | | |
| K149-4 | 34 | .2005 | 2000 | .0328 | 18.6 | 9.9 | 10.4 | 692 | .45 | -1.0 | 44.6 | 43.1 | 21.1 | -22.0 | 40.2 | 28.5 | -11.7 | .41 | .04 | | 2193 | 2733 | 5602.7 | A.B. |
| (RELAXED VALUES) | | | | | | | | | | | | 48.5 | | -19.4 | 34.8 | | -6.3 | .35 | .10 | .12 | | | | |

NOTES: A PLASTIC STRAIN SHUTDOWN; B: FAILED IN GAGE; R: RUNOUT; N#/2 VALUES TAKEN AT TERMINATION OF TEST.
0 INDICATES THE VALUE IS NOT AVAILABLE - SEE FOOTNOTE, REMARK AND/OR FOLLOWING DATA LINE FOR FURTHER EXPLANATION.

MAR-TEST [illegible] 5184
DCT [illegible]



Copy available to DTIC does not permit fully legible reproduction

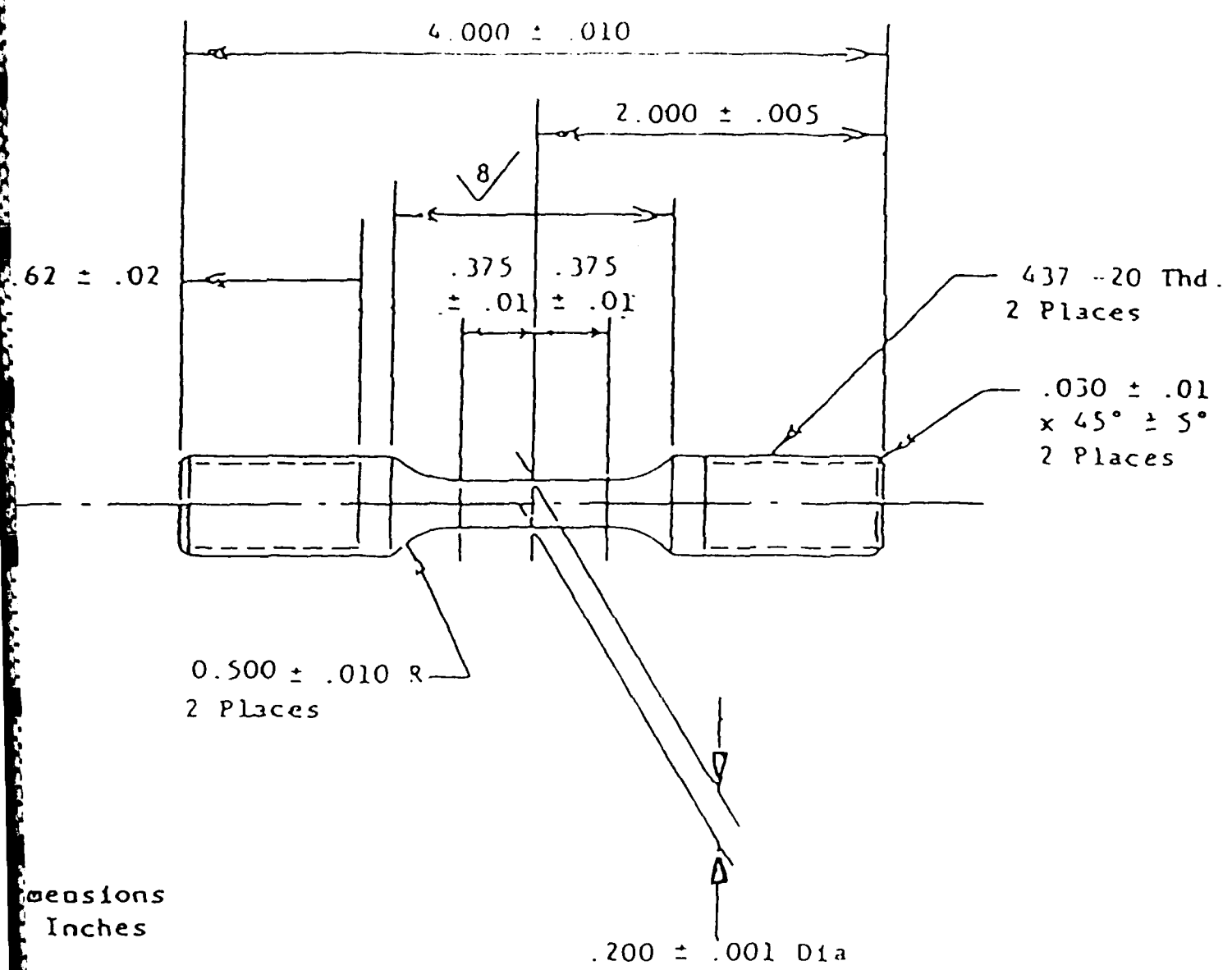


Figure 1 Axial LCF/GCF Test Specimen

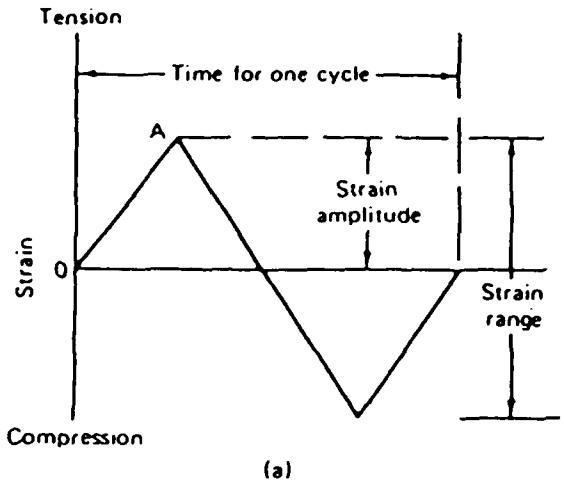


(a)

[1] Triangular with hold period (on strain) in compression only.

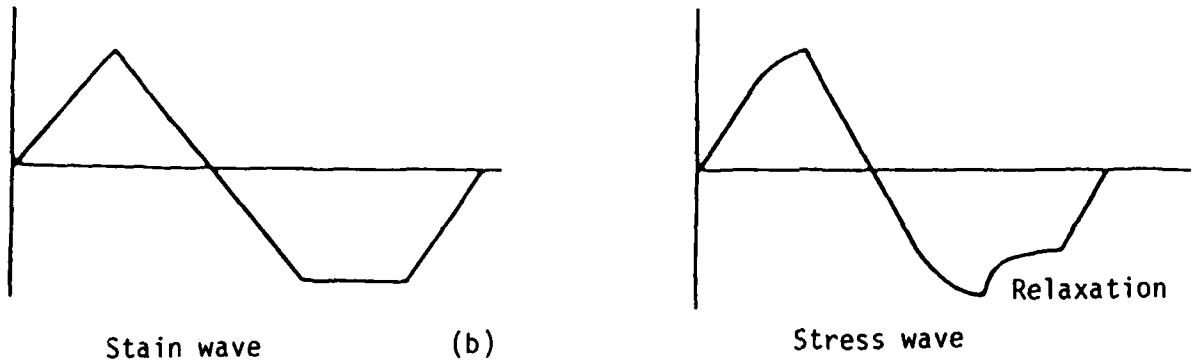


Stain wave (b) Stress wave

Figure 2 Strain Wave Forms Used

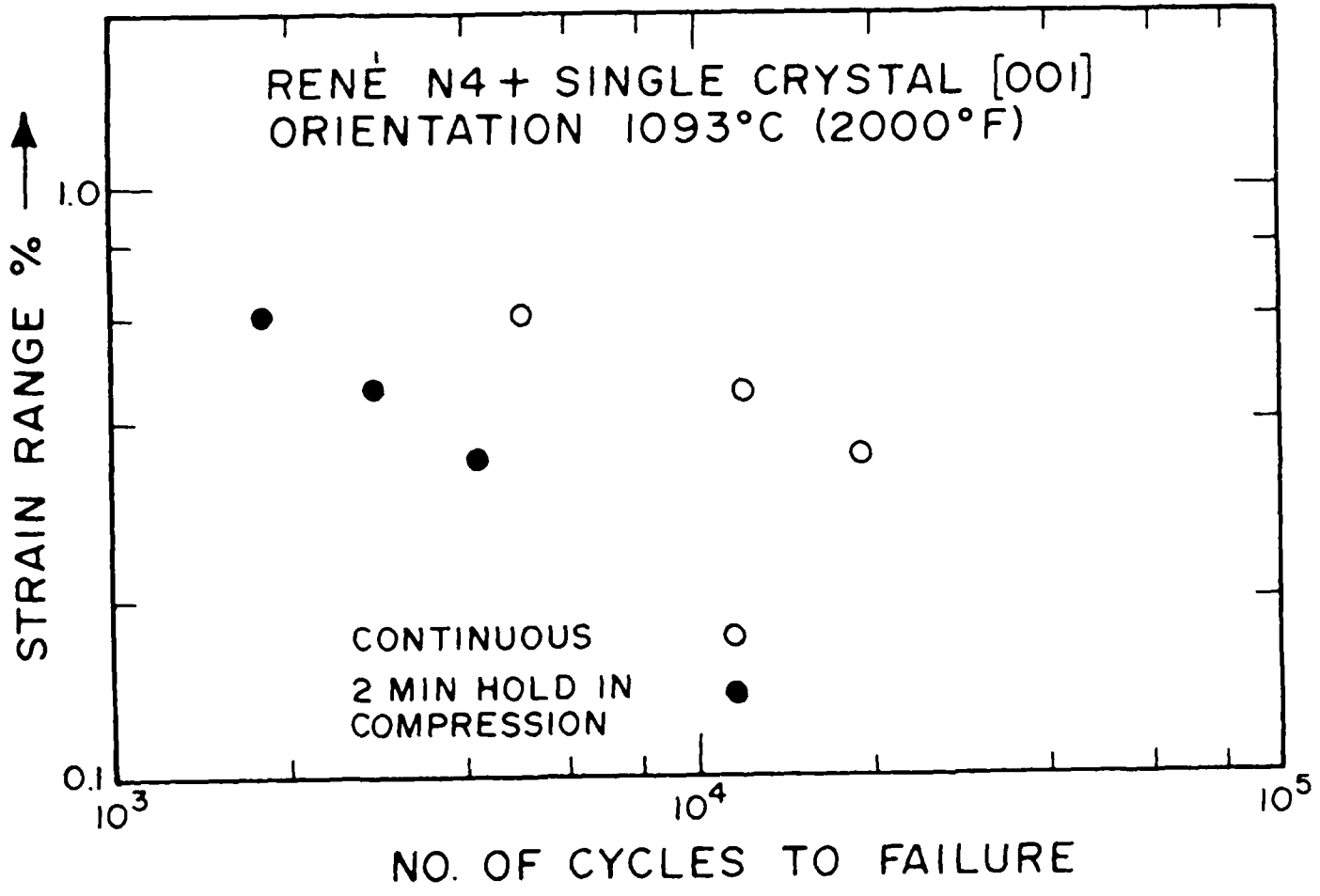


Figure 3 Relationship Between Strain Range and No. of Cycles to Failure

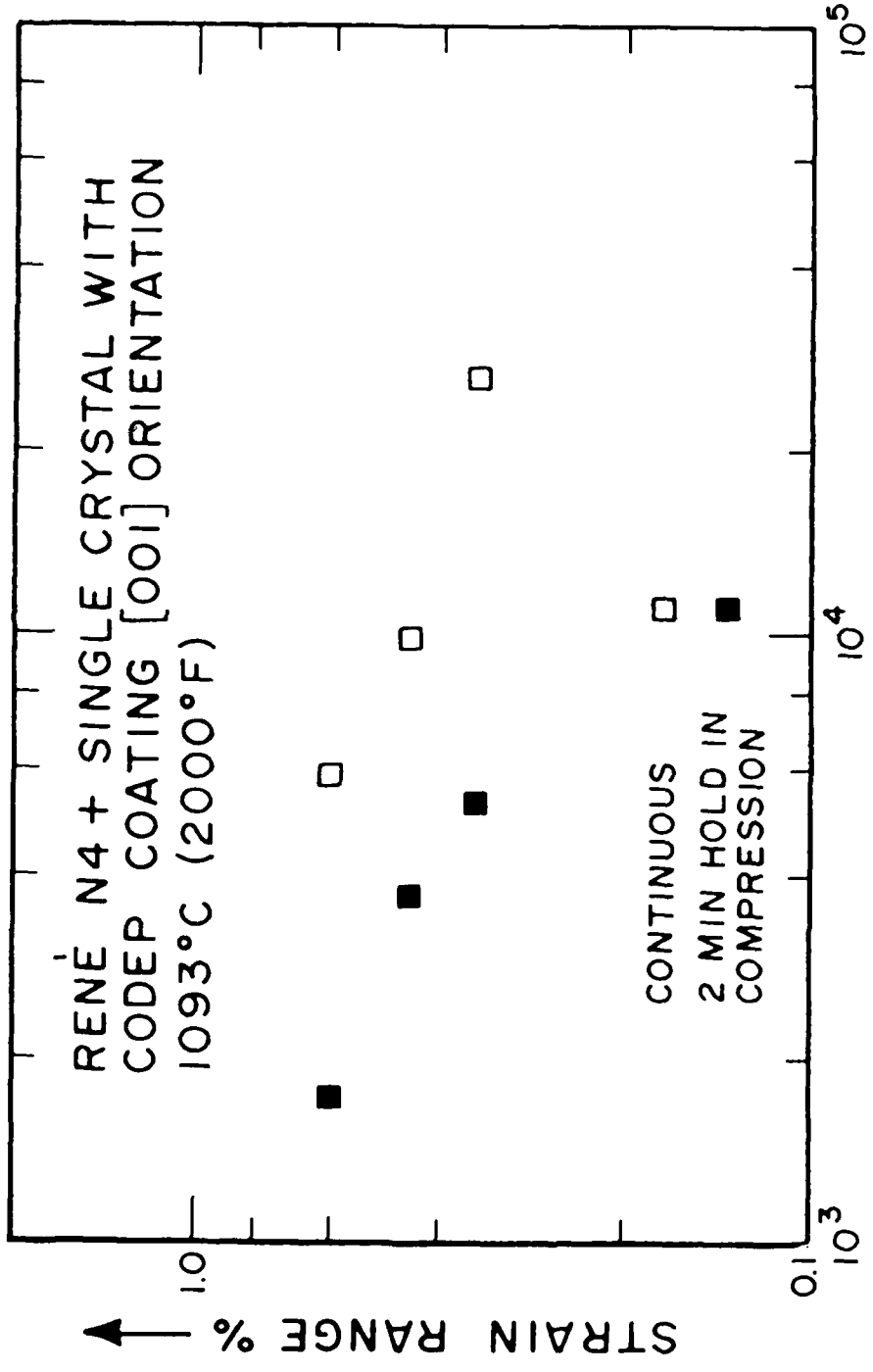


Figure 4 Relationship Between Strain Range and No. of Cycles to Failure

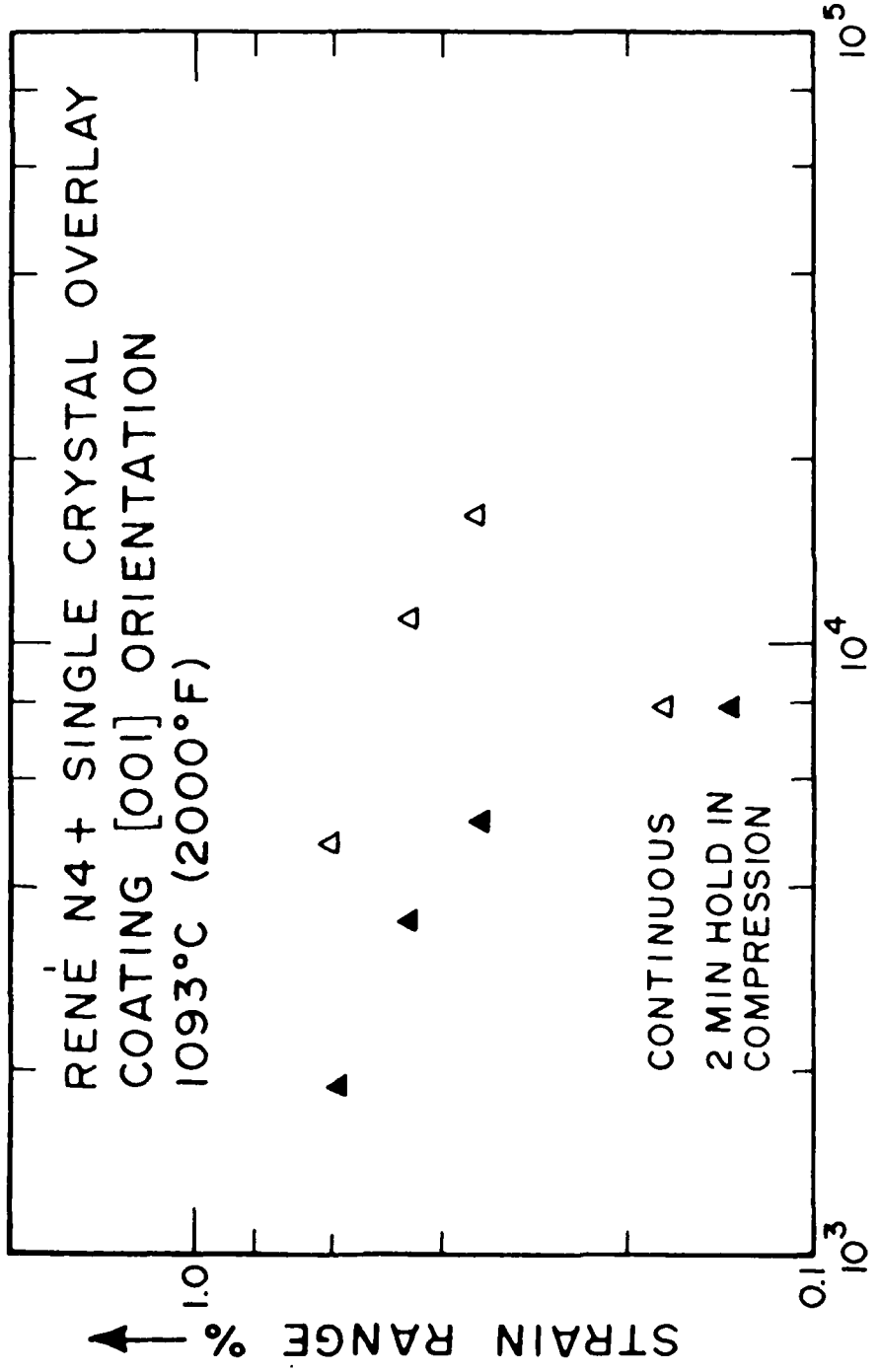


Figure 5 Relationship Between Strain Range and No. of Cycles to Failure

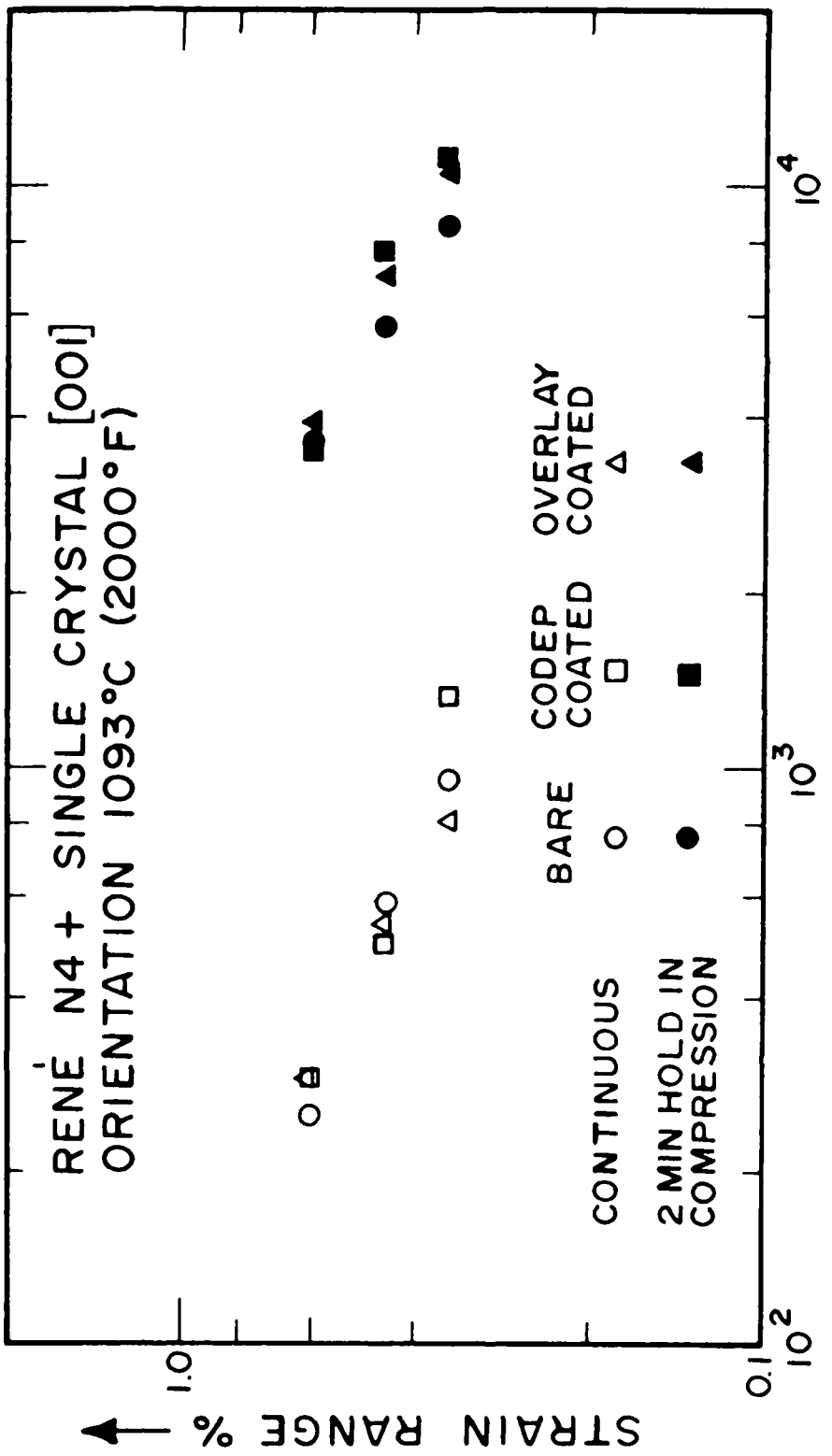


Figure 6 Relationship Between Strain Range and No. of Cycles to Failure

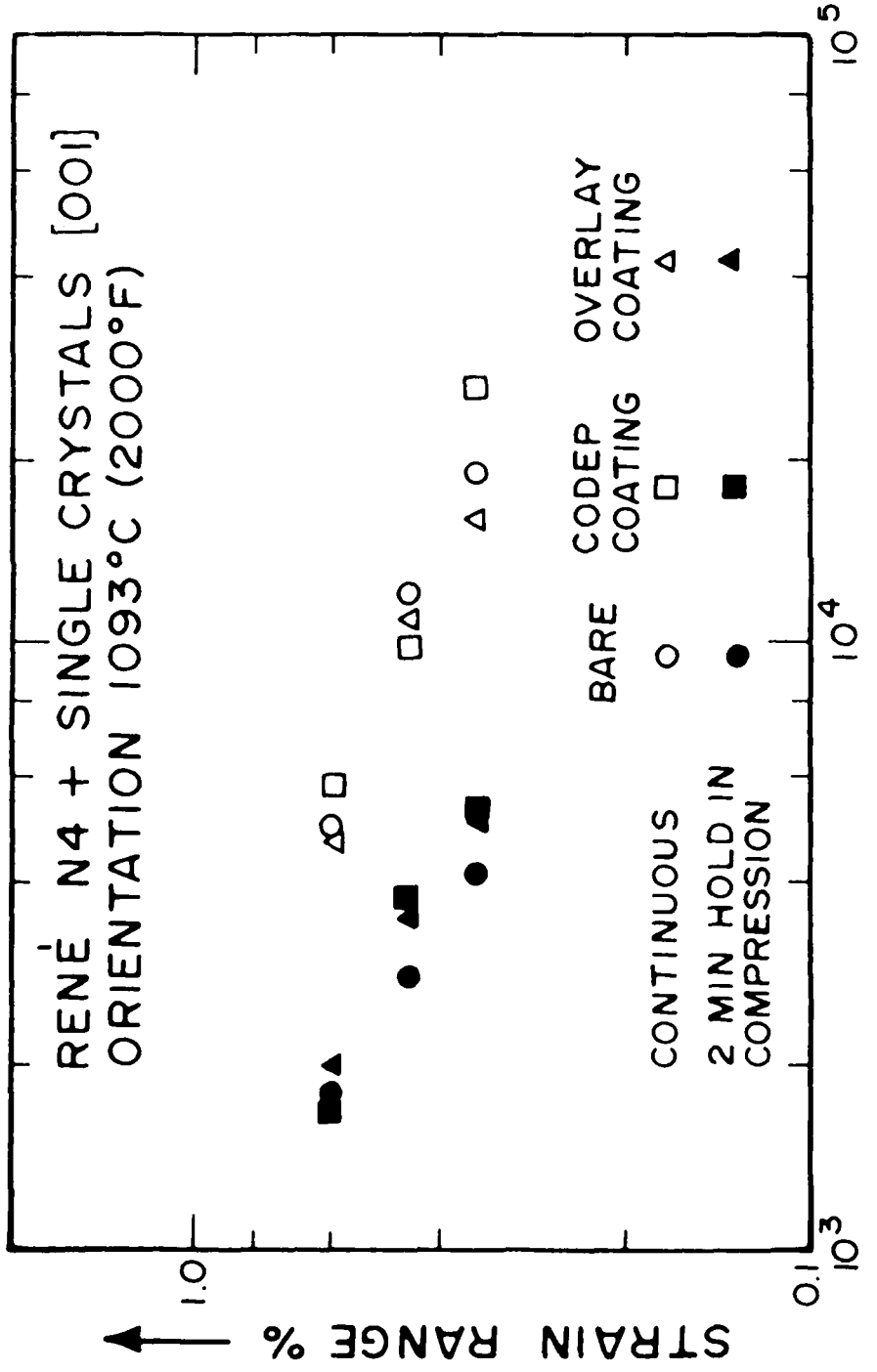


Figure 7 Relationship Between Strain Range and Time to Failure

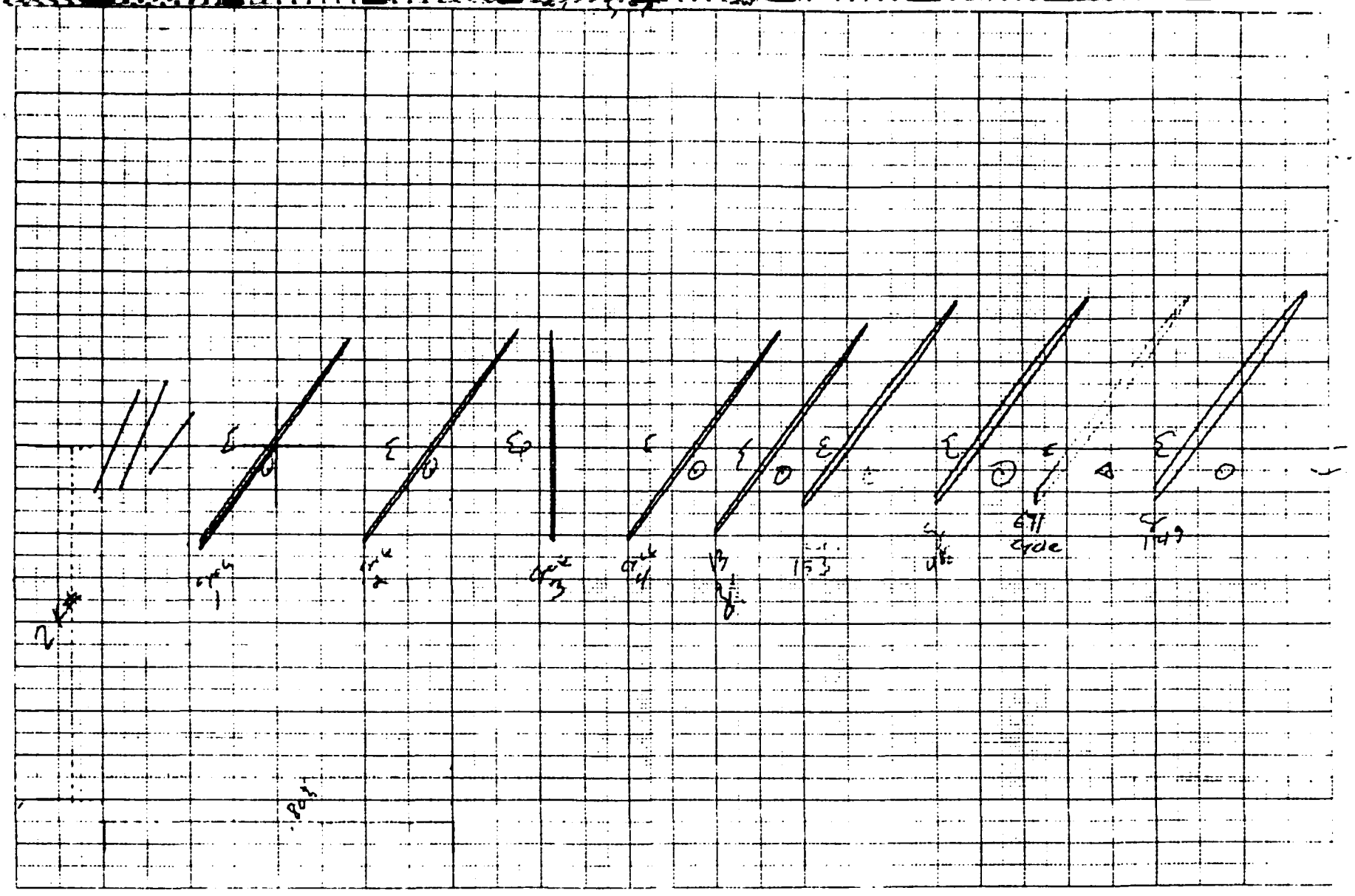

Figure 8 Hysteresis Loops, (K 149 - 2)

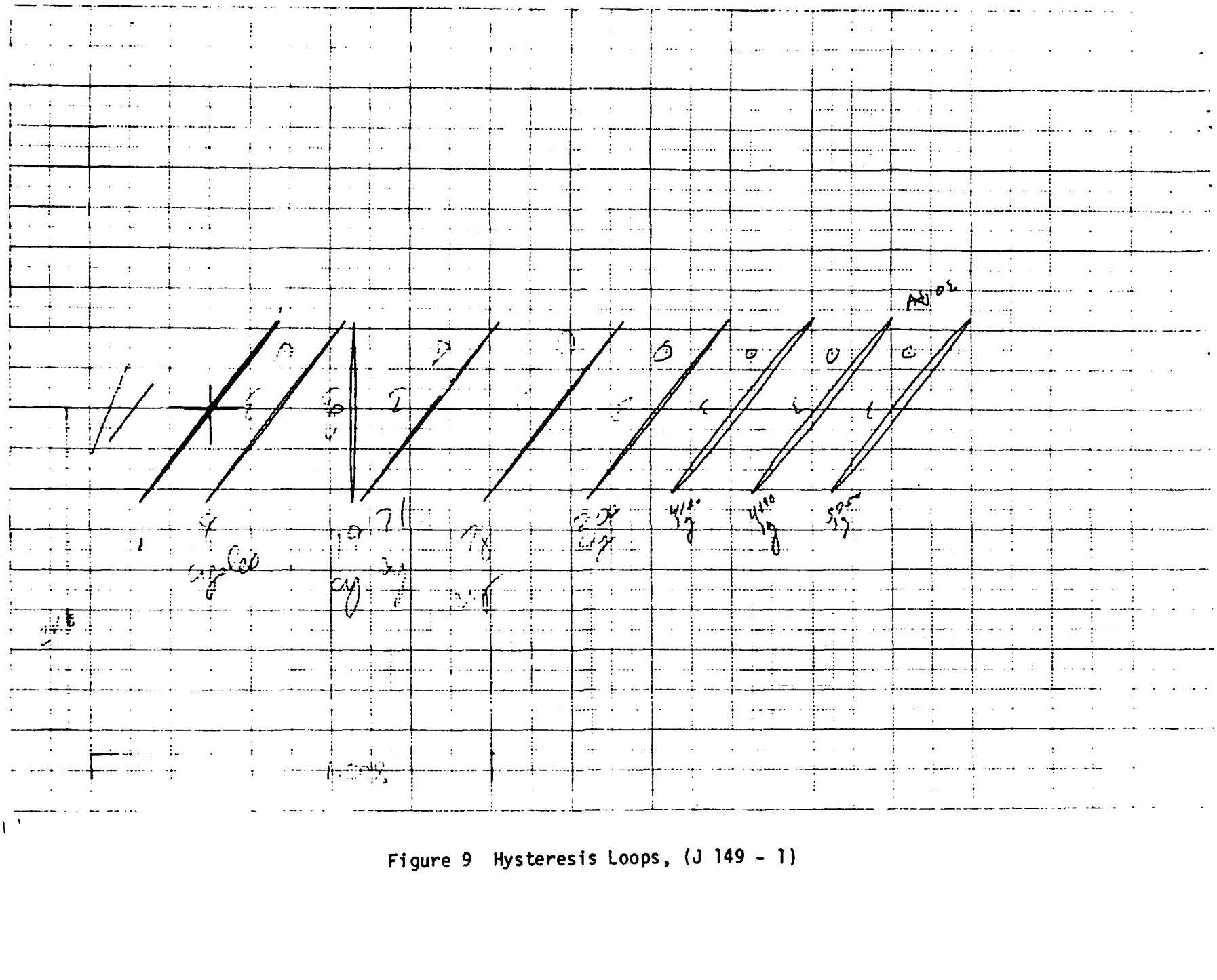

Figure 9 Hysteresis Loops, (J 149 - 1)

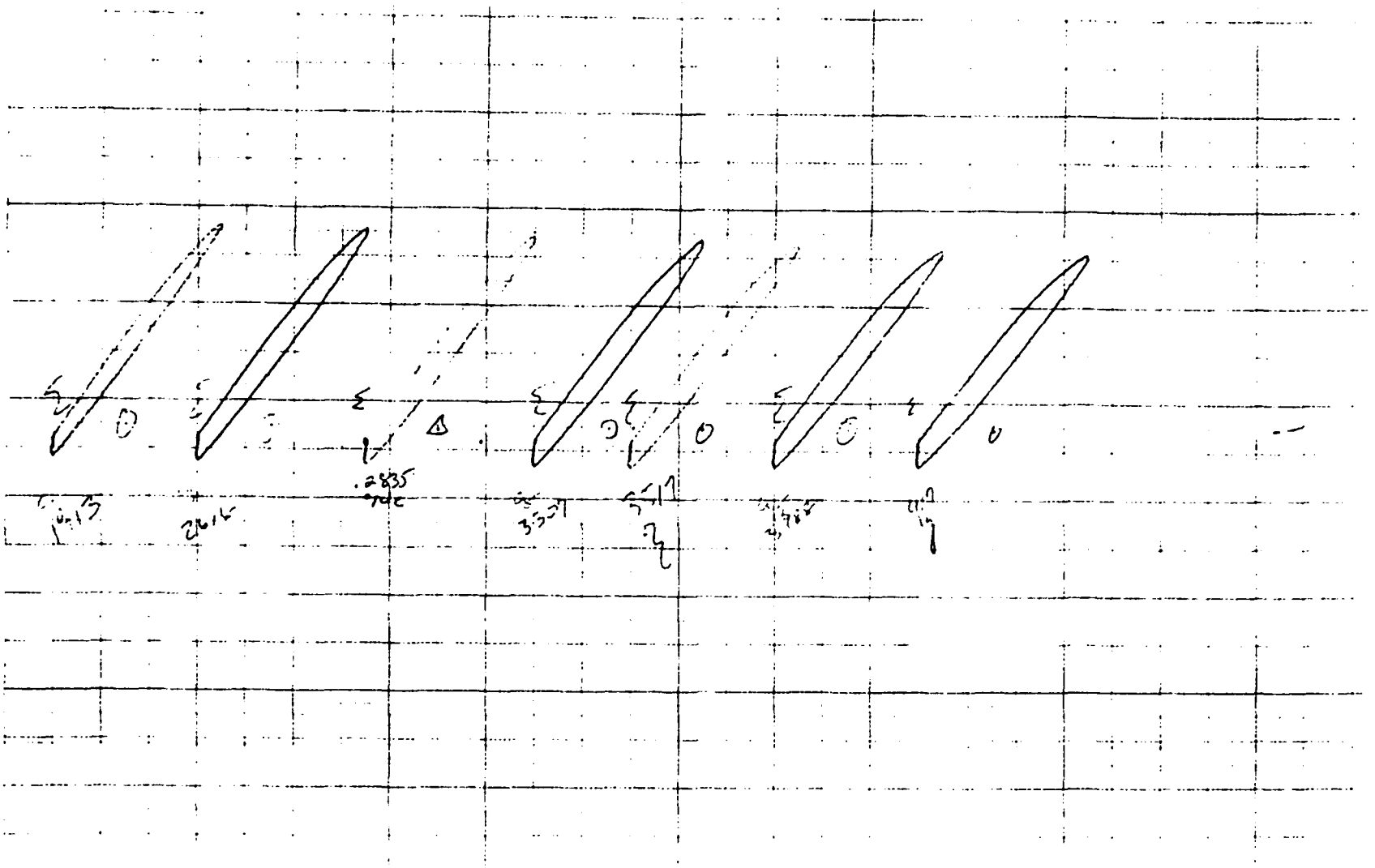

Figure 9 Hysteresis Loops, (J 149 - 1) Continued

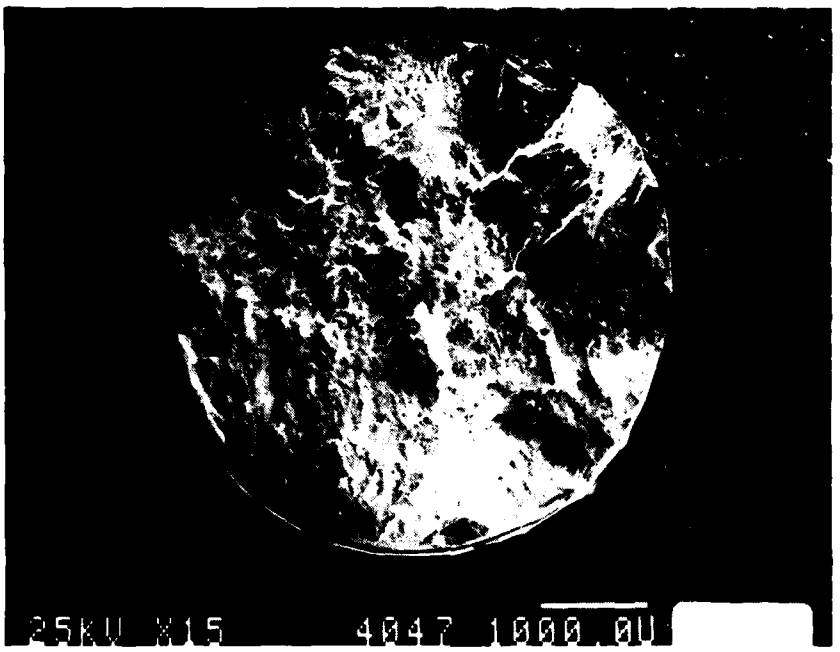


L 151-1 a

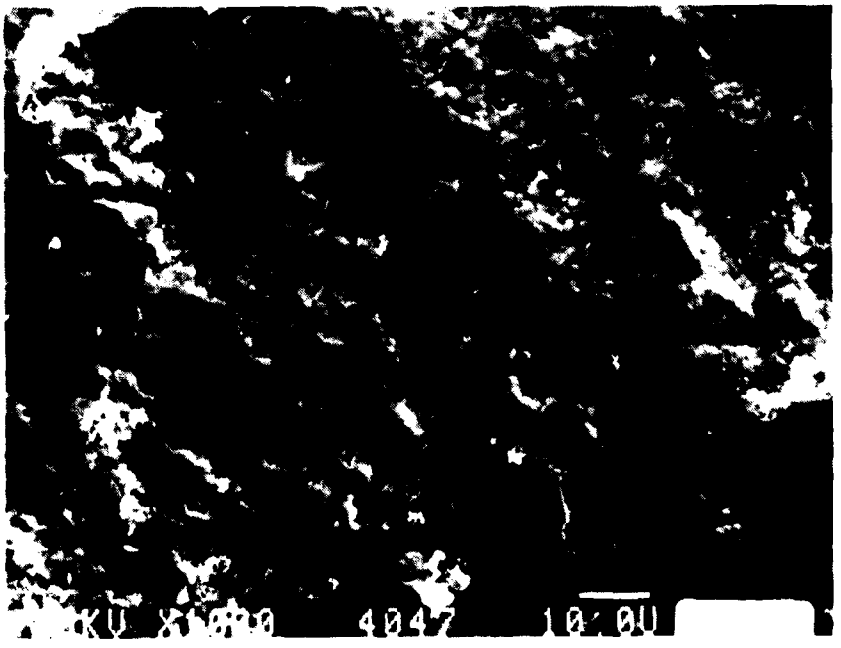

L151-1 b

FIGURE 10 Fracture Surfaces

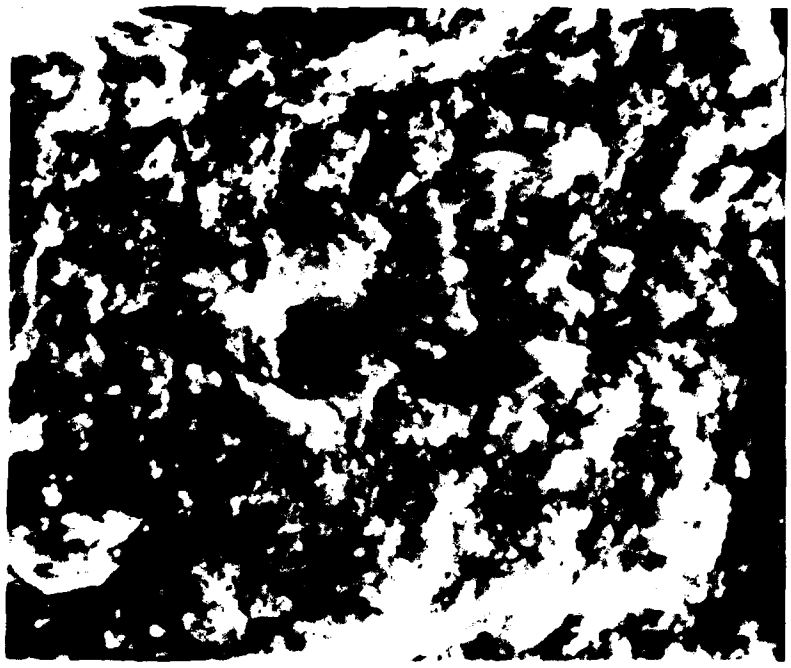

L151-1 a MAG 1500X

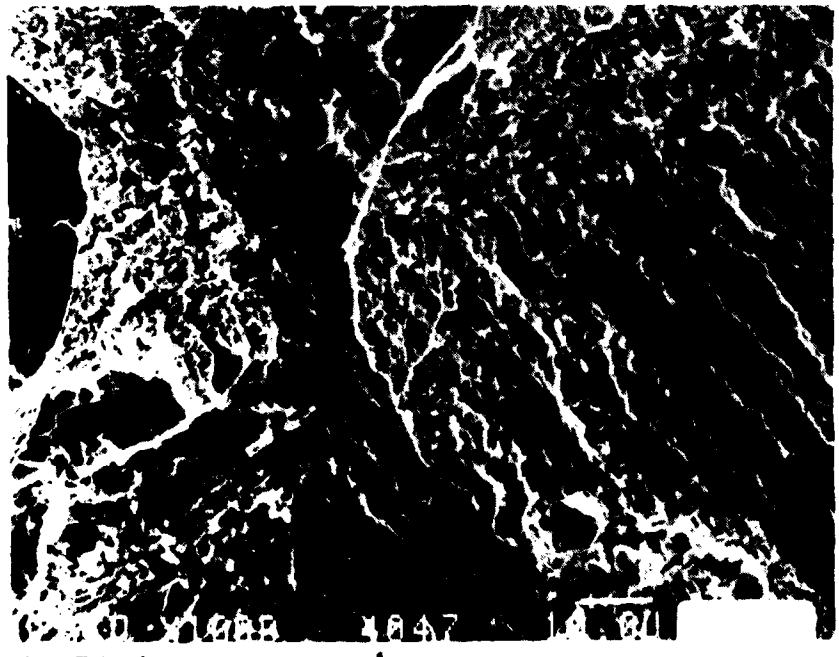

L151-1 b

FIGURE 11 Fracture Surfaces

E151-2 a

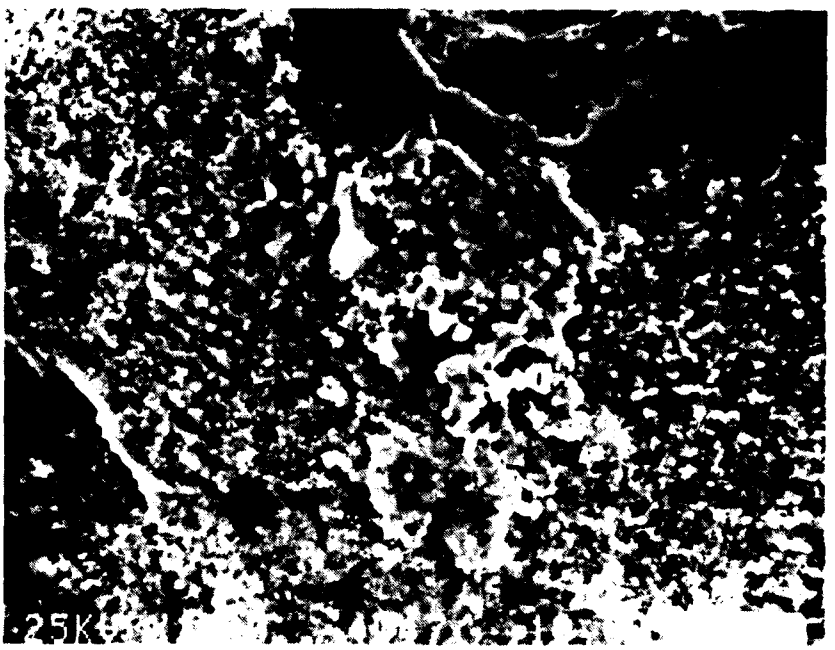


E151-2 b

FIGURE 12 Fracture Surfaces

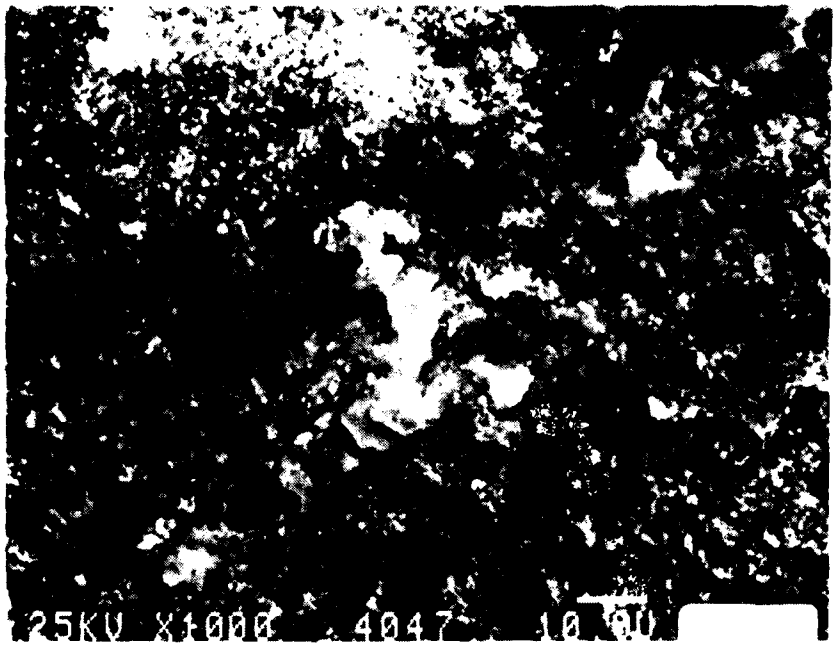


E 151-2 a

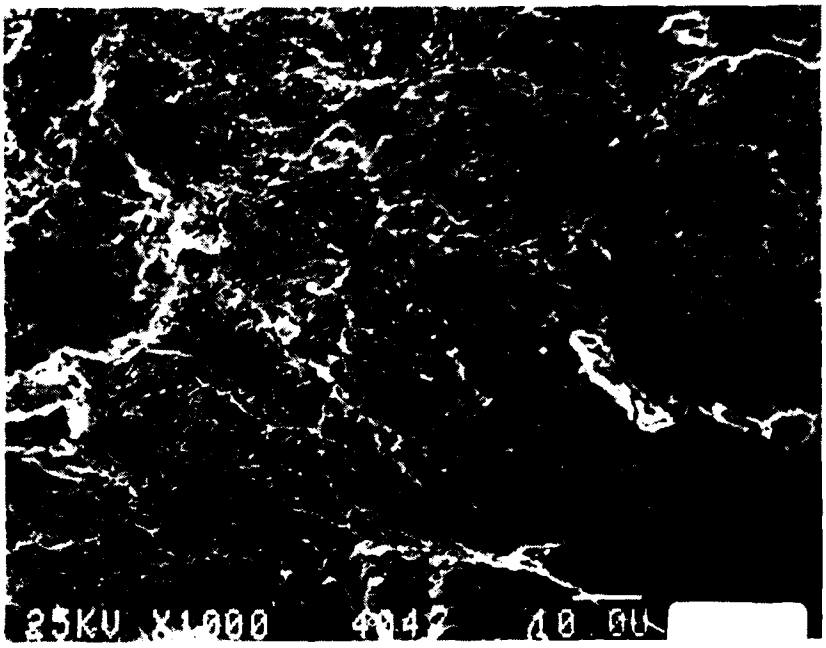


E 151-2 b

FIGURE 13 Fracture Surfaces

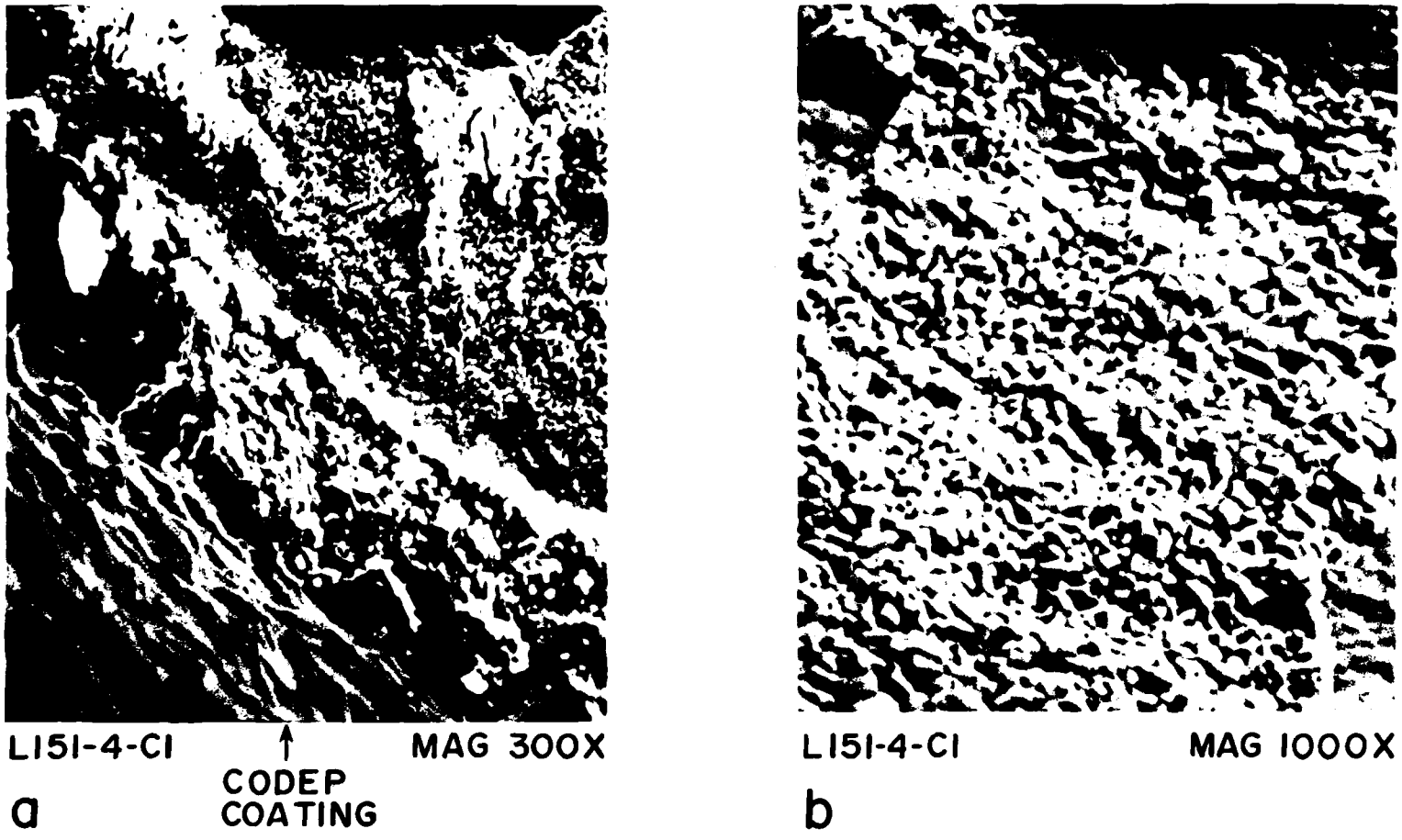


FIGURE 14 Fracture Surfaces

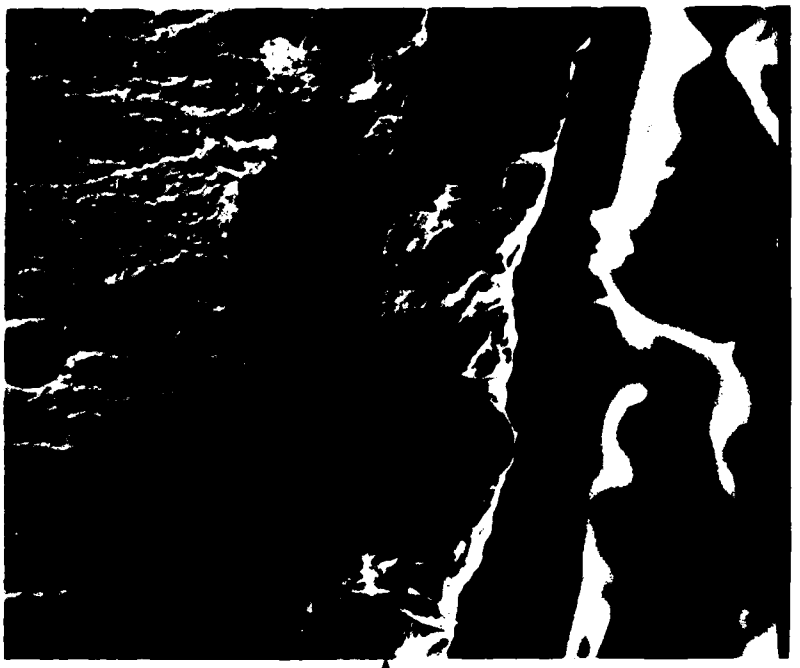


a

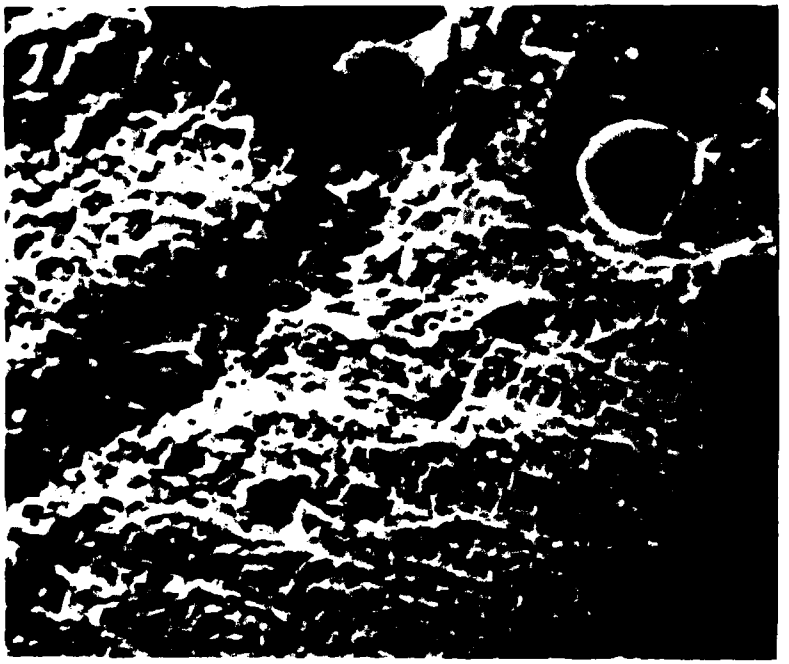


b

FIGURE 15 Fracture Surfaces

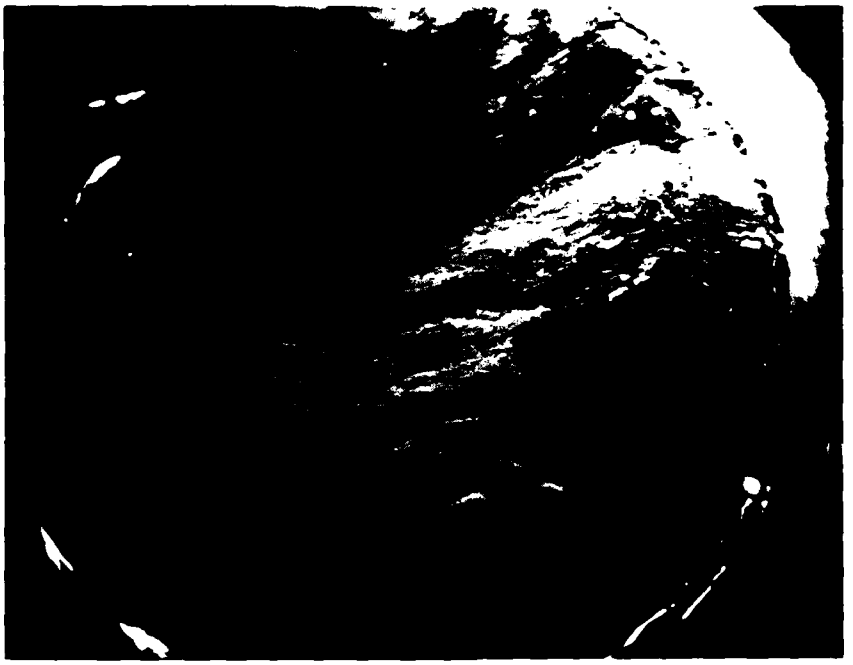

K149-3-C1 MAG 20X

a

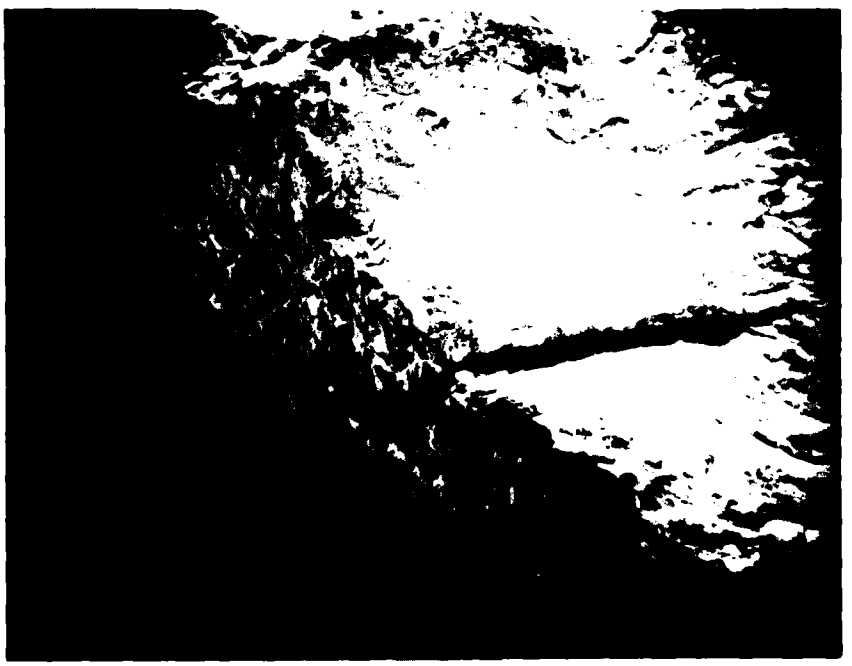

K149-3-C1 MAG 100X

b

FIGURE 16 Fracture Surfaces

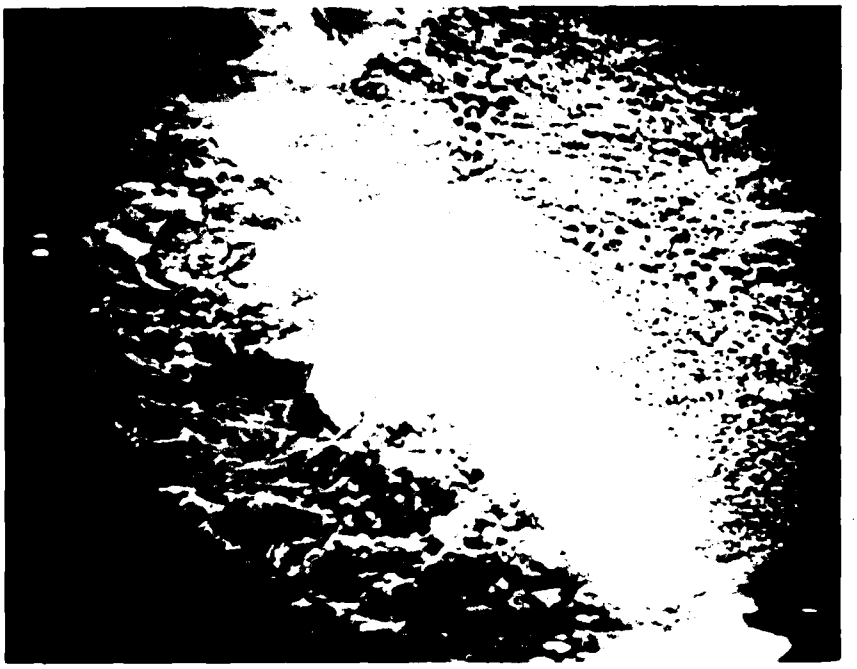

K149-3-CI a MAG 500X

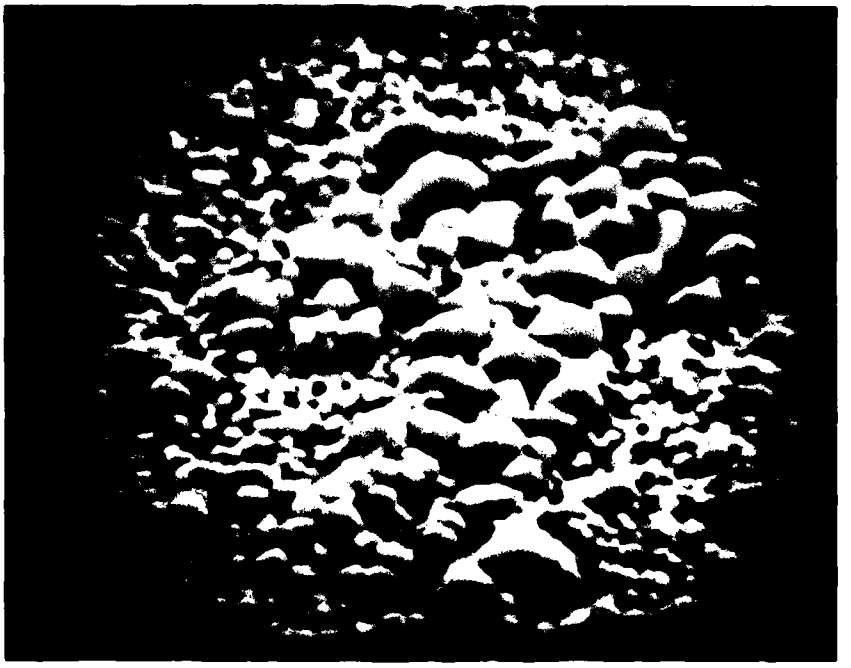

K149-3-CI b MAG 1960X

FIGURE 17 Fracture Surfaces

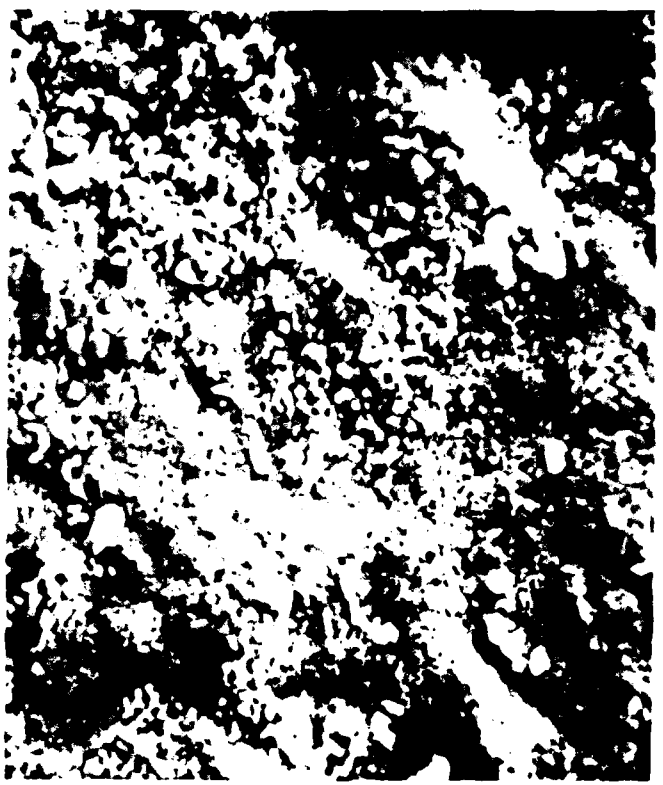


FIGURE 18 Fracture Surfaces

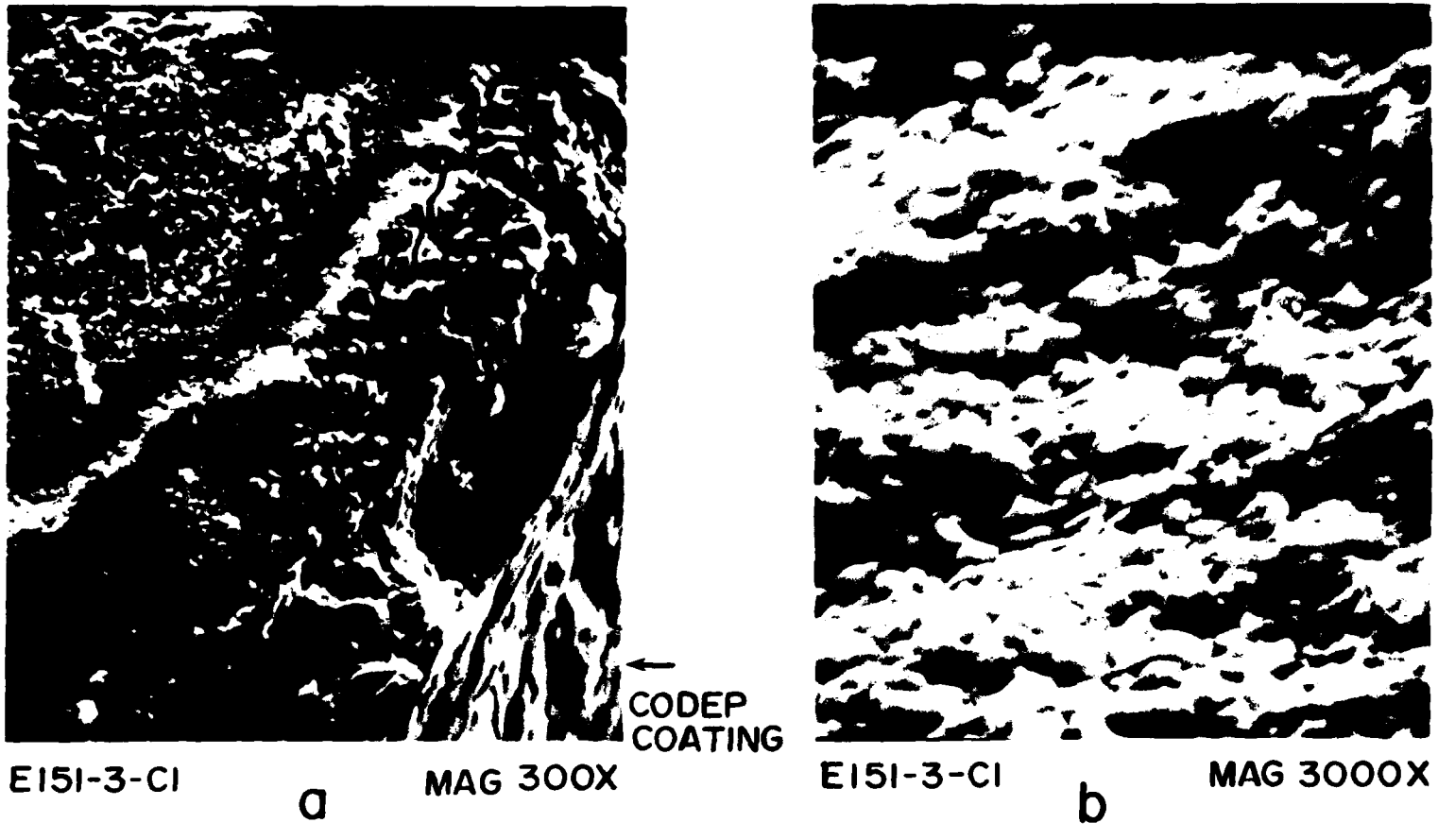


FIGURE 19 Fracture Surfaces

K149-2 a MAG 150X

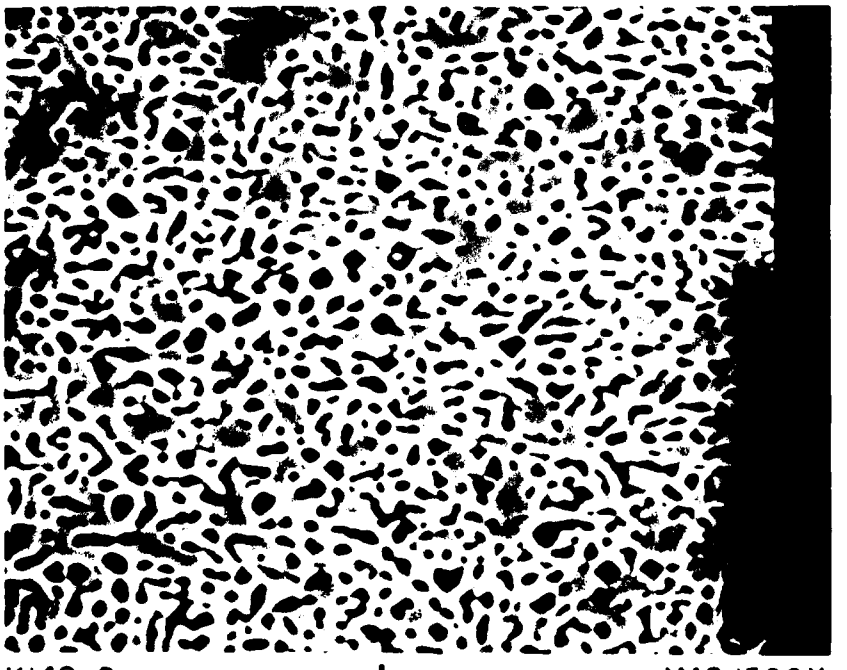


K149-2 b MAG 1500X

FIGURE 20 Polished and Etched Longitudinal Section

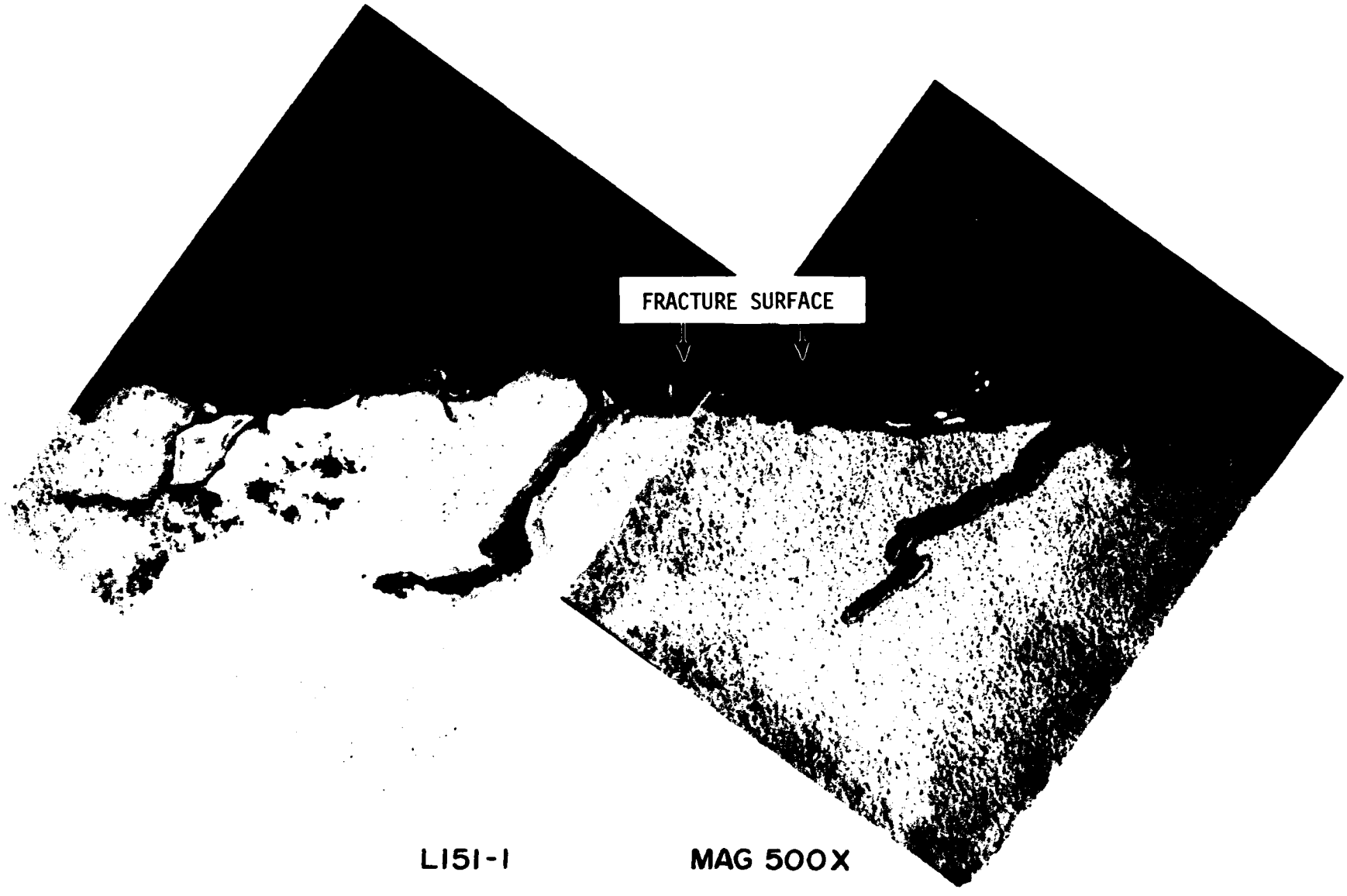


FIGURE 21 Polished and Etched Longitudinal Section

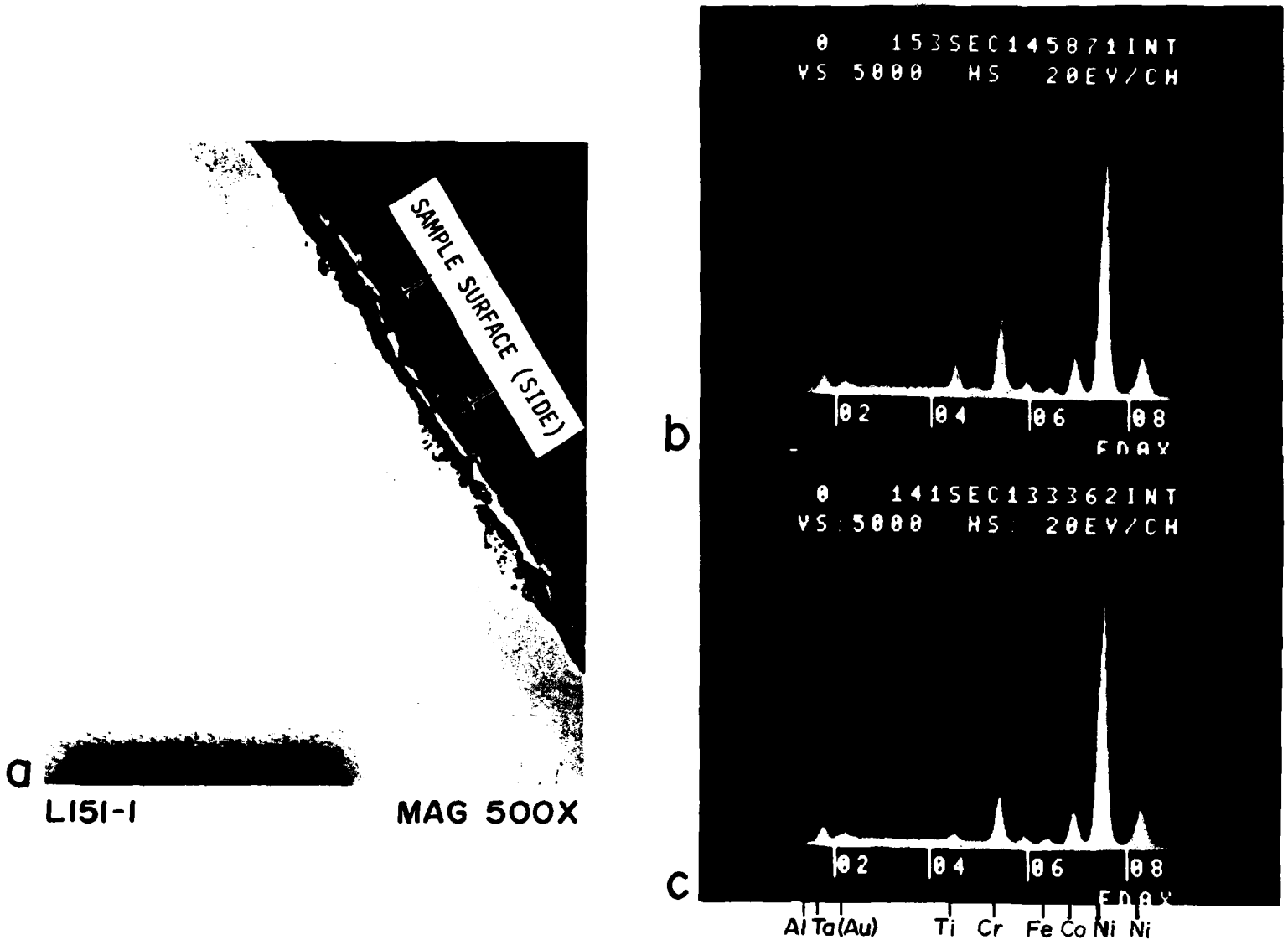


Figure 22 (a) Polished and Etched Longitudinal Section
(b,c) EDAX Spectra from the Interior and the Edge Respectively

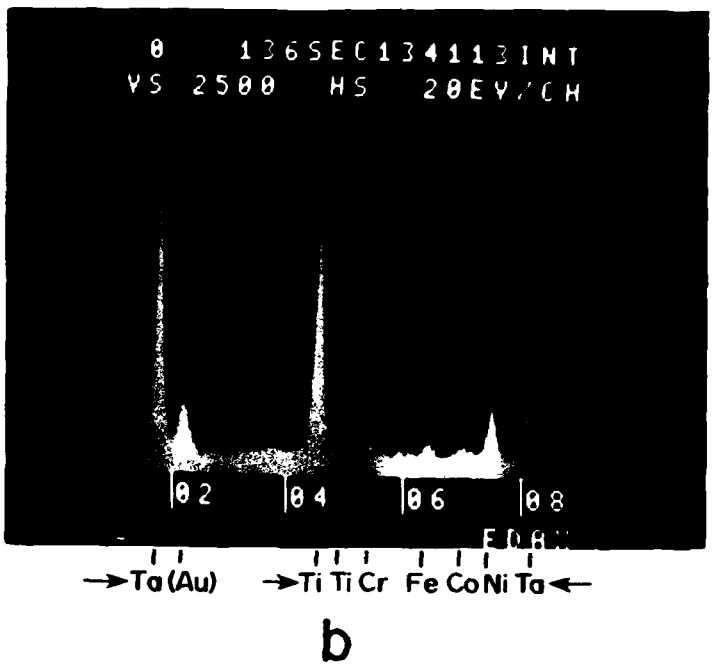


FIGURE 23(a) Particles
(b) EDAX Spectrum of the Particles

FIGURE 24 Polished and Etched - Longitudinal Sections

E151-2 a MAG 150X

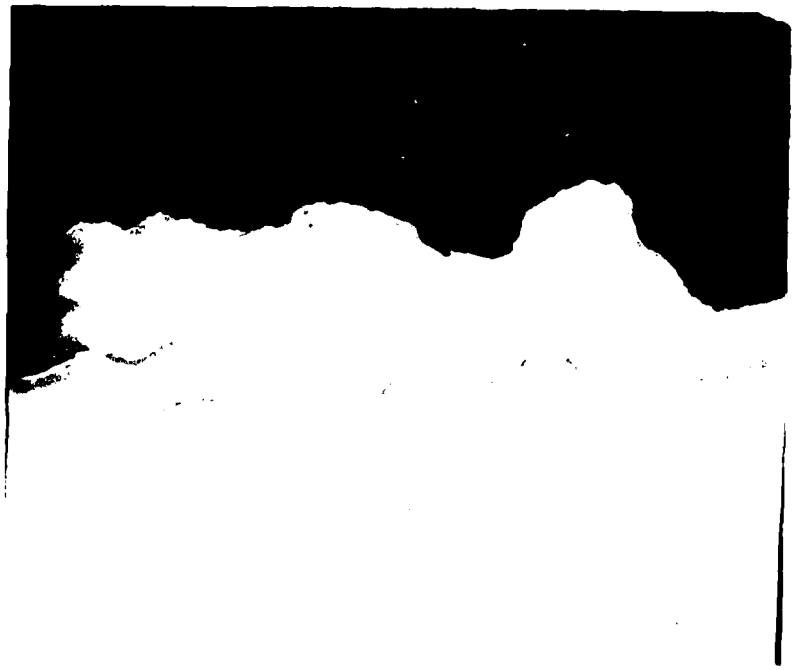

E151-2 b MAG 150X

FIGURE 25 Polished and Etched Longitudinal Sections Near the Fracture Surface

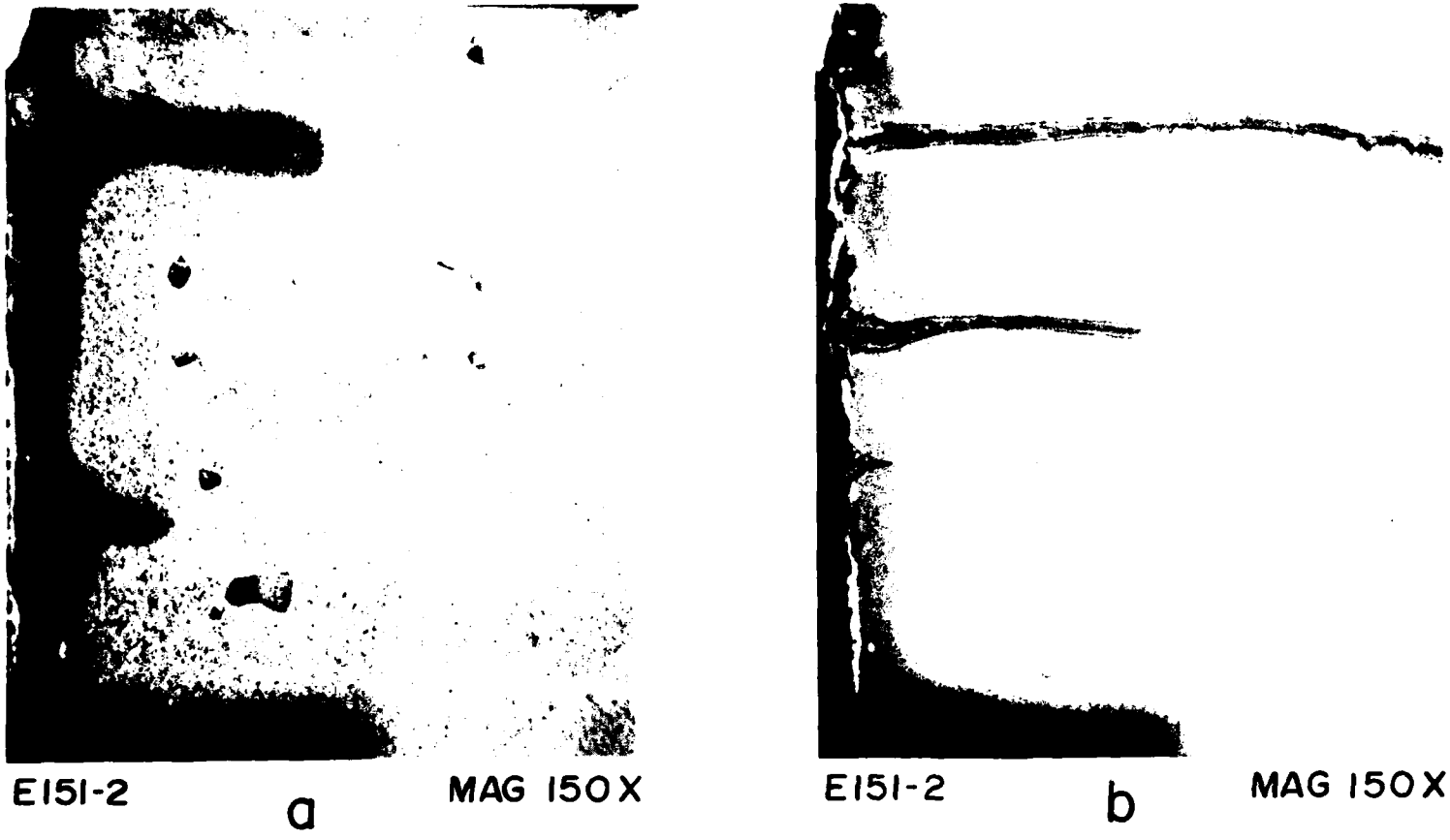


FIGURE 26 Polished and Etched Longitudinal Section

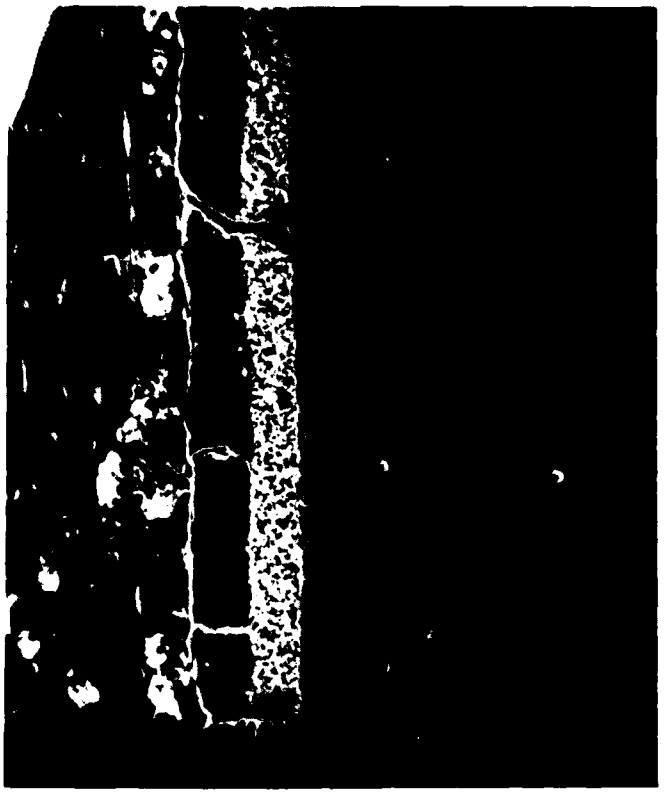

J149-4-C1 a MAG 150X

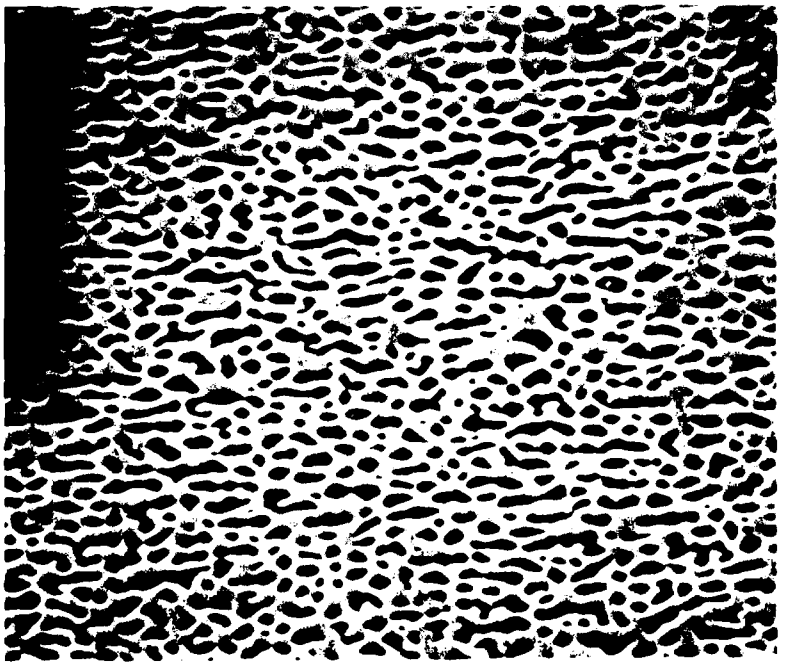


J149-4-C1 b MAG 1500X

FIGURE 27 Polished and Etched Longitudinal Section

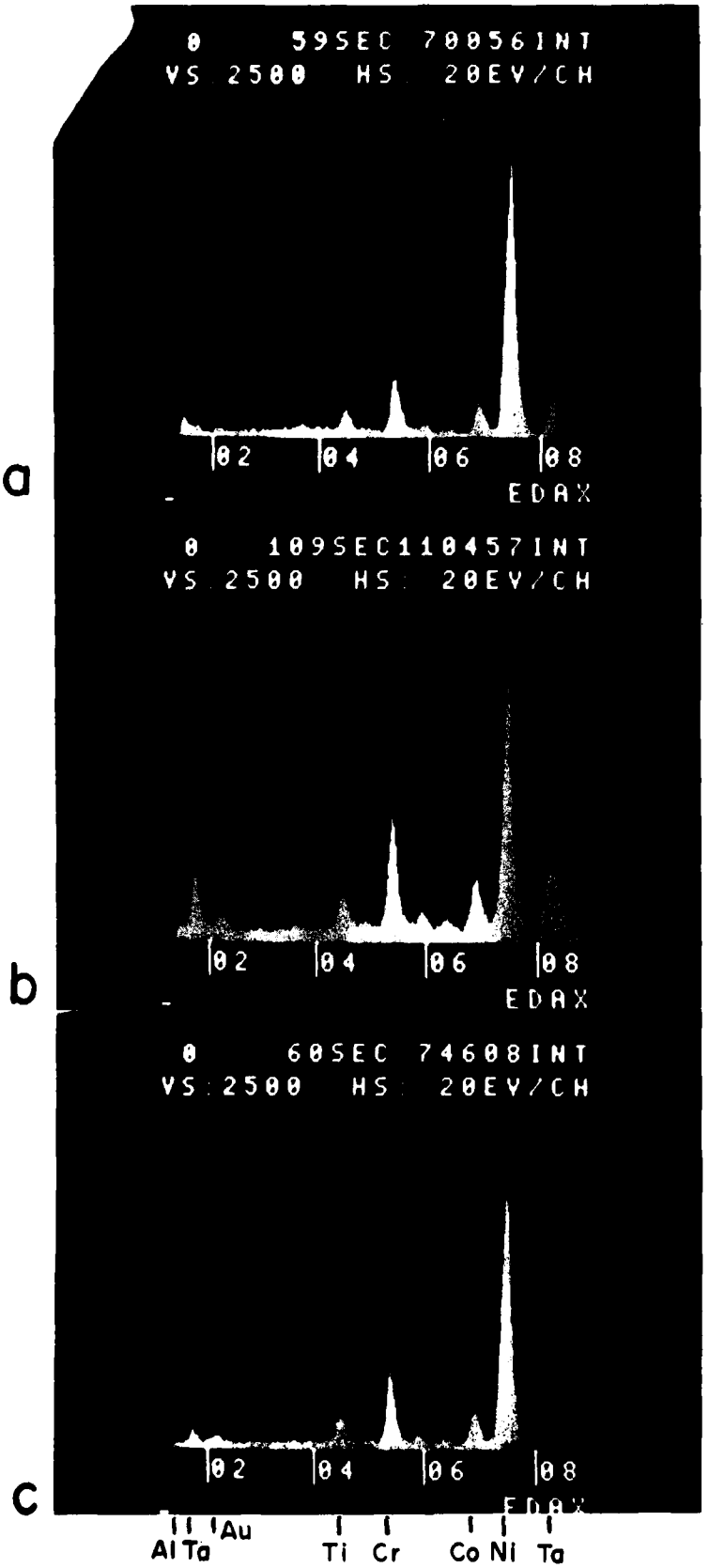


J149-4-C1

FIGURE 28 EDAX Spectra from (a) Coating
(b) The Diffusion Zone
(c) The Interior

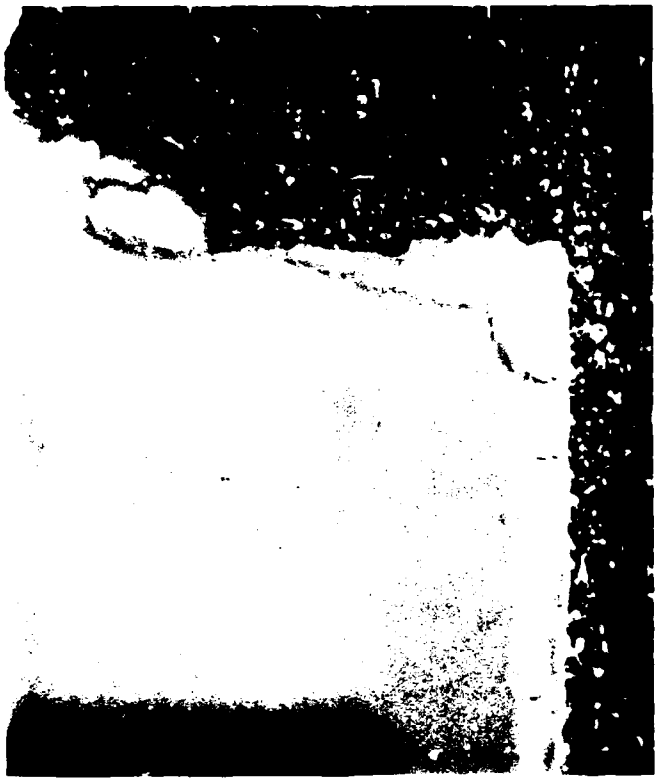

FIGURE 29 Polished and Etched Longitudinal Sections near the Fracture

E151-3-C1 a MAG 150X

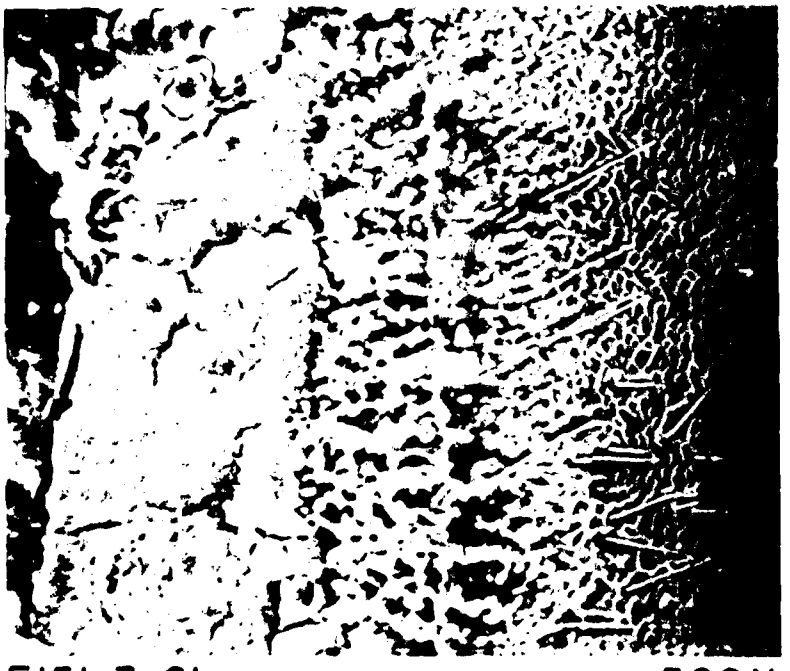

E151-3-C1 b 500X

FIGURE 30 Polished and Etched Longitudinal Sections

E151-3-C1 a MAG 50X

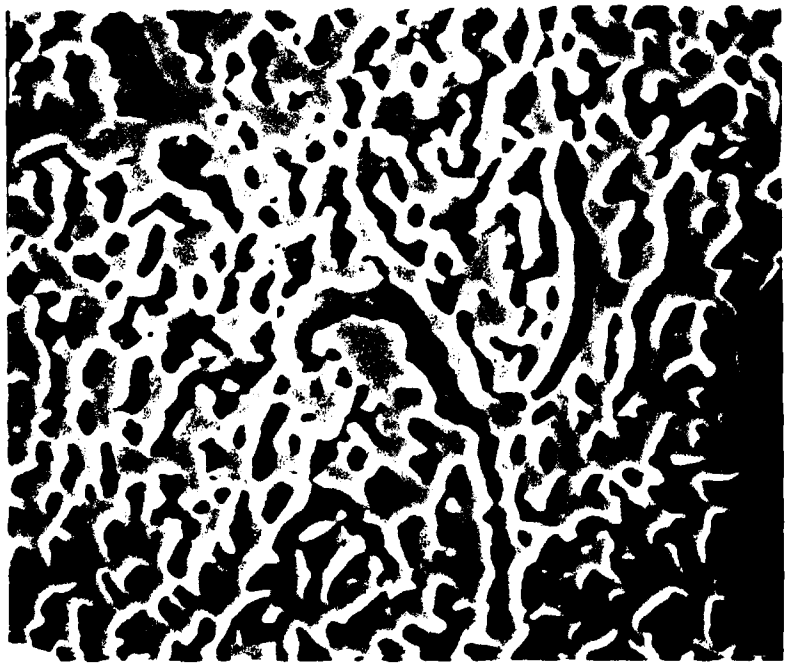



E151-3-C1 b MAG 1500X

FIGURE 31 Polished and Etched Longitudinal Sections

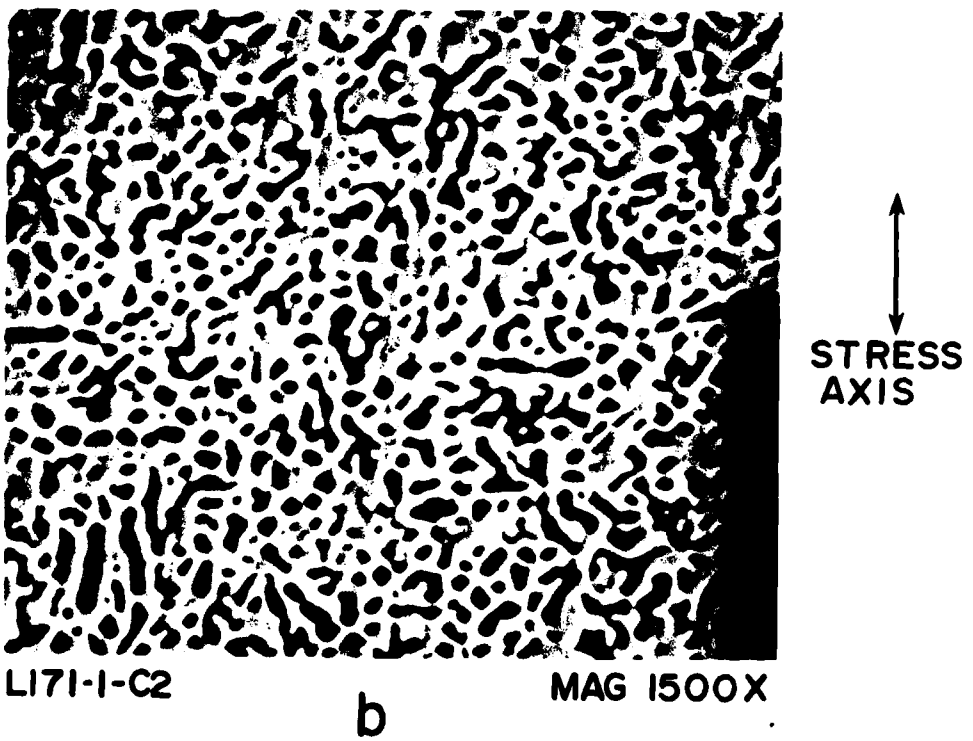


FIGURE 32 Polished and Etched Longitudinal Sections

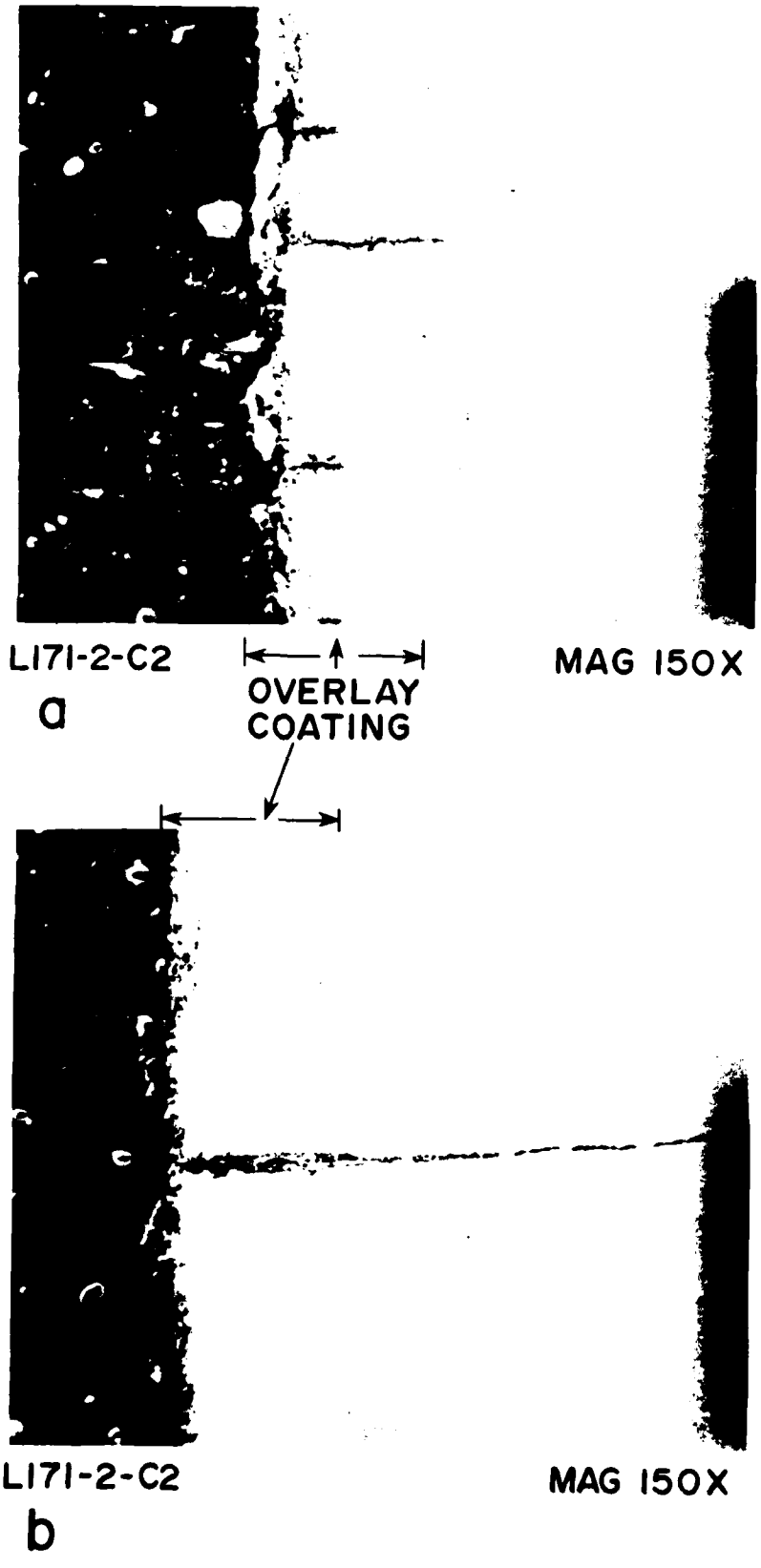


FIGURE 33 Polished and Etched Longitudinal Sections

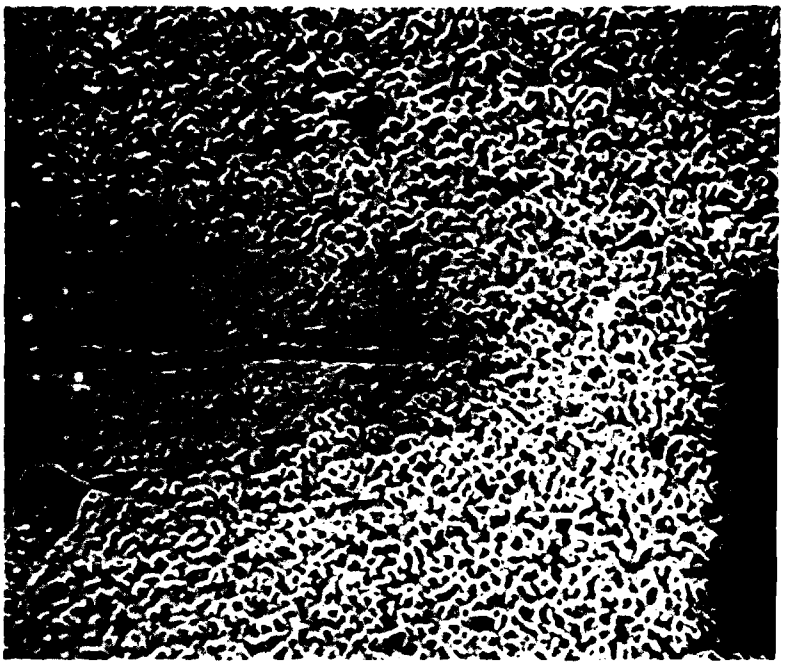

L171-2-C2 a MAG 150X

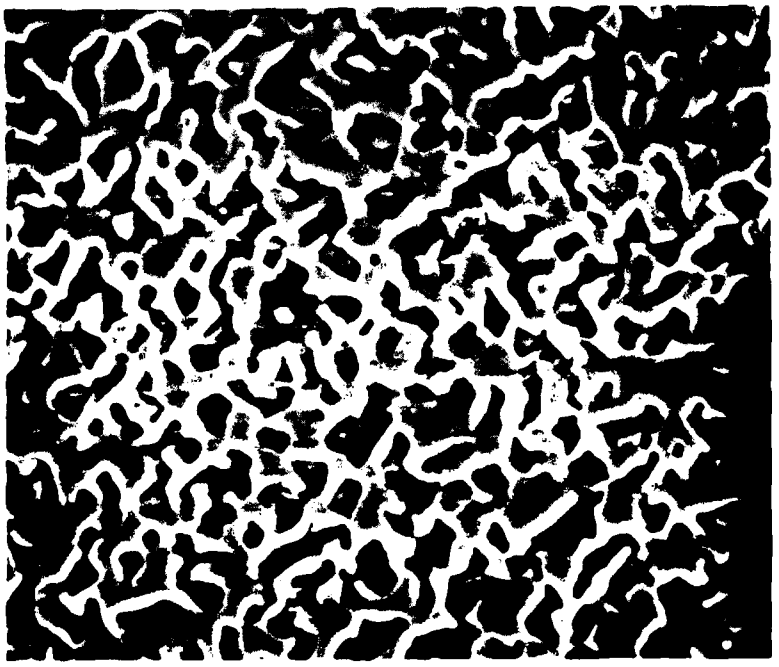

L171-2-C2 b 1500X

FIGURE 34 Polished and Etched Longitudinal Sections

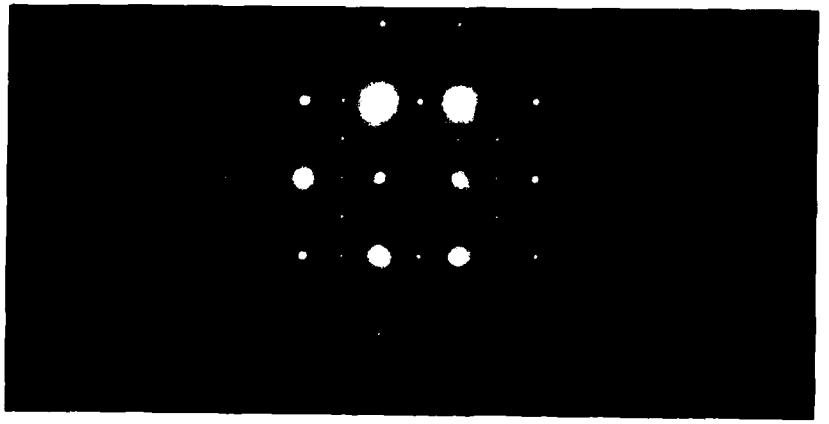

a

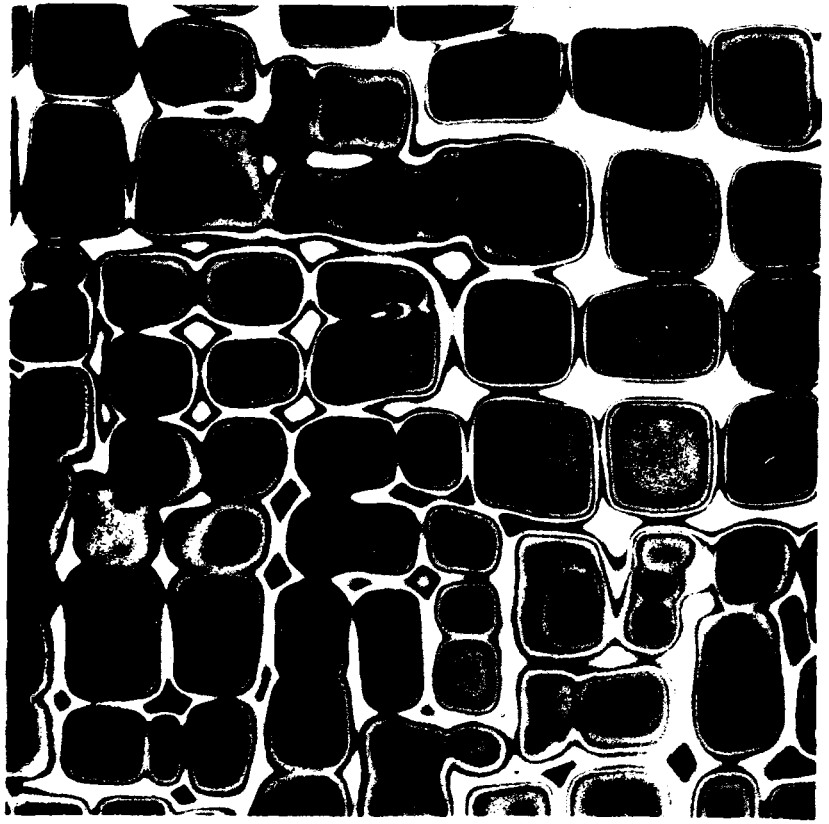

b

c

FIGURE 35(a) Electron Diffraction Pattern, (b) Bright Field and (c) Dark Field Images

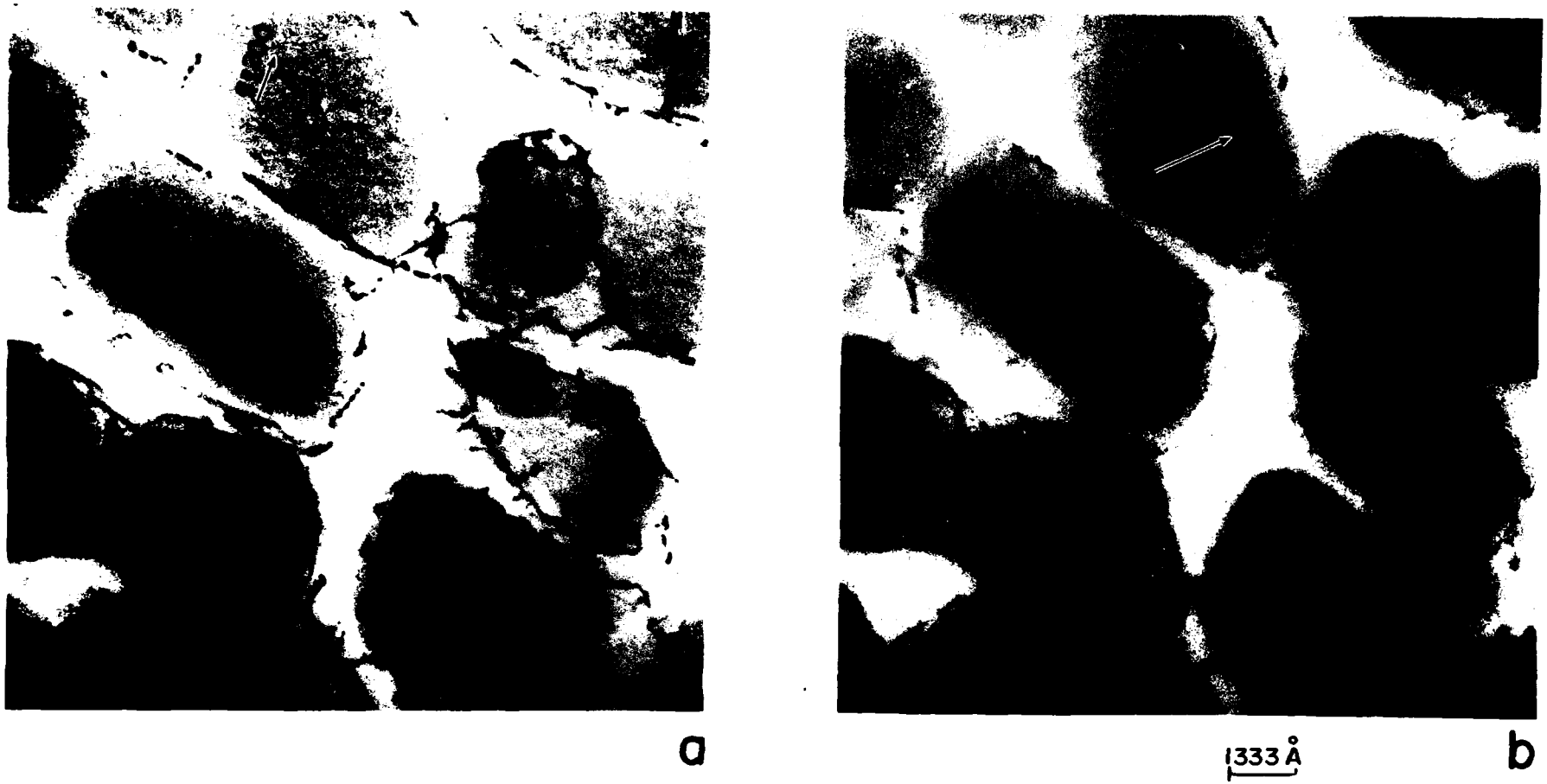


FIGURE 36 Transmission Electron Micrographs with Different $\vec{g}$ Vectors

FIGURE 37 Transmission Electron Micrograph

FIGURE 38 Transmission Electron Micrograph

L151-1

MAG 75000X

FIGURE 39 Transmission Electron Micrograph

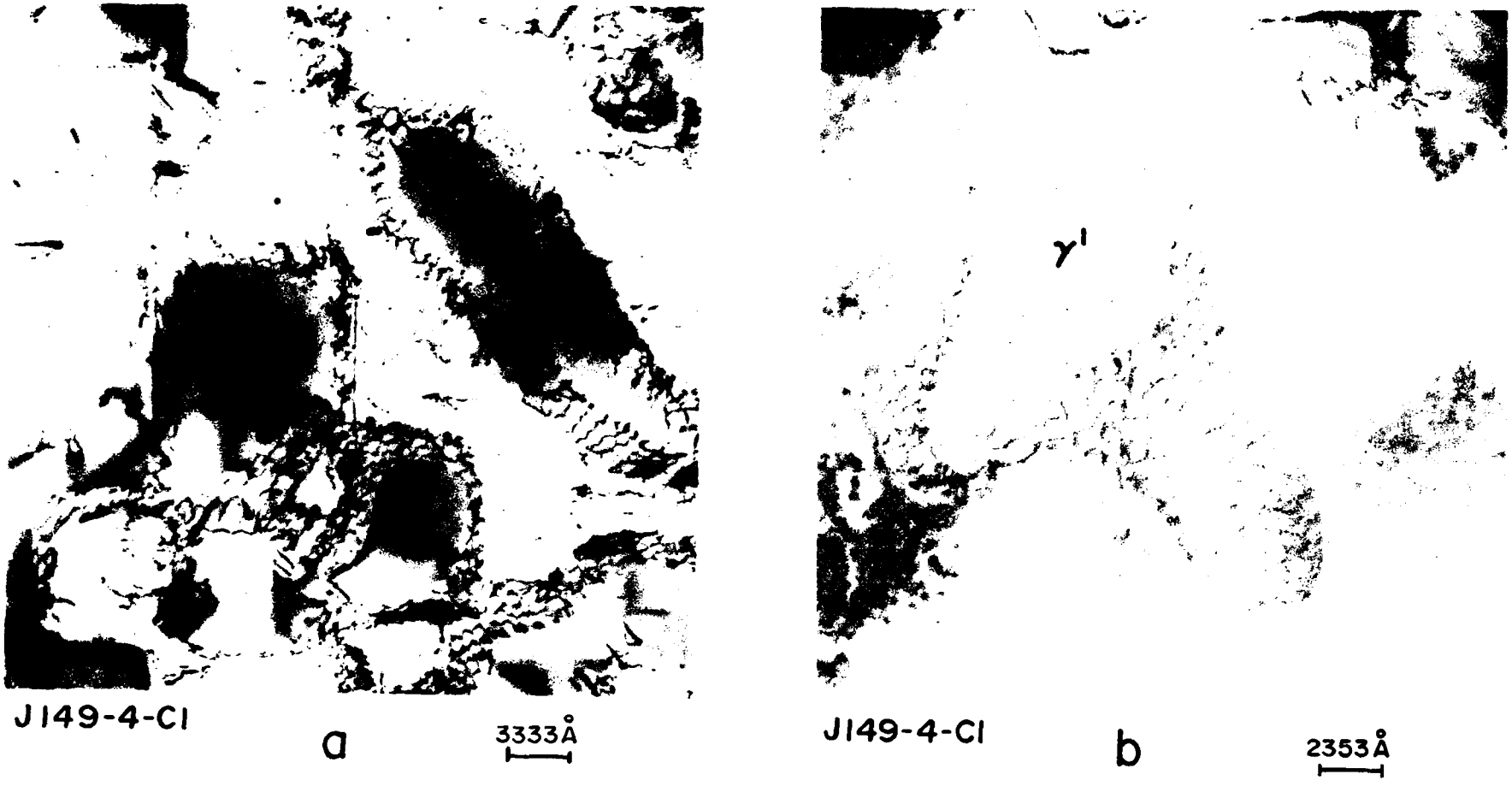


FIGURE 40 Transmission Electron Micrograph

FIGURE 41 Transmission Electron Micrograph

FIGURE 42 Transmission Electron Micrograph

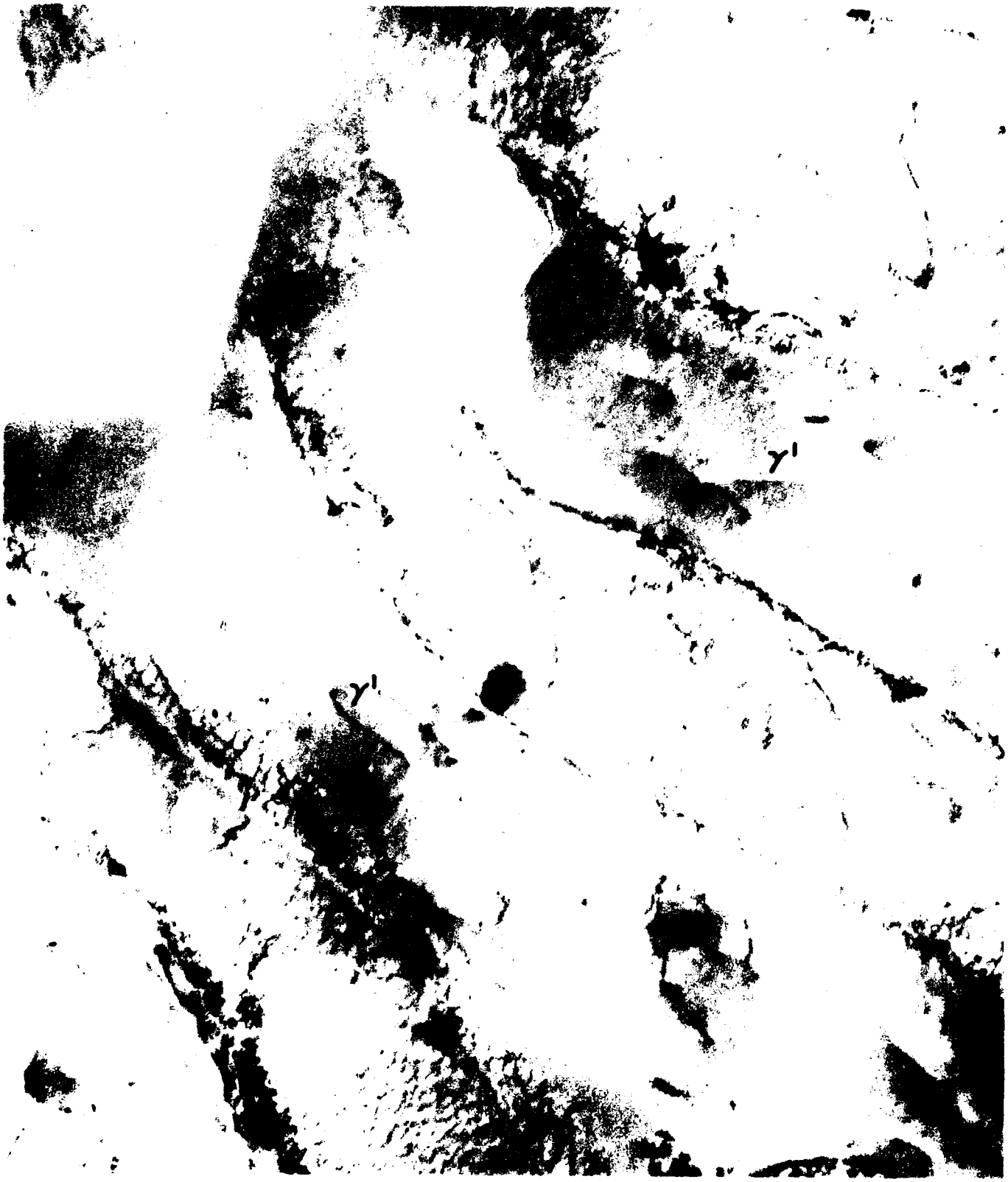


FIGURE 43 Transmission Electron Micrograph

FIGURE 44 Transmission Electron Micrograph

FIGURE 45 Replica Electron Micrograph

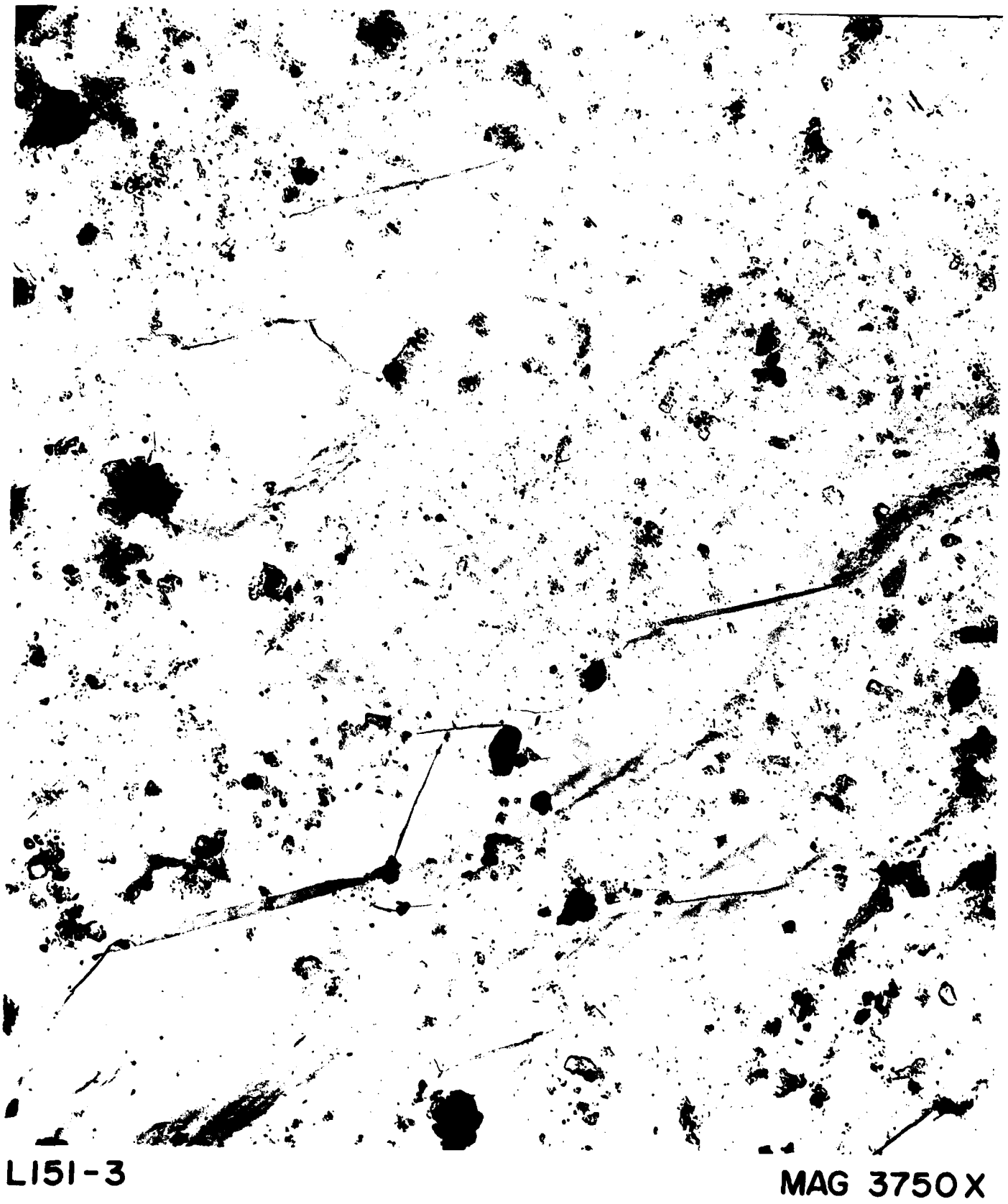


FIGURE 46 Replica Electron Micrograph

FIGURE 47 Replica Electron Micrograph

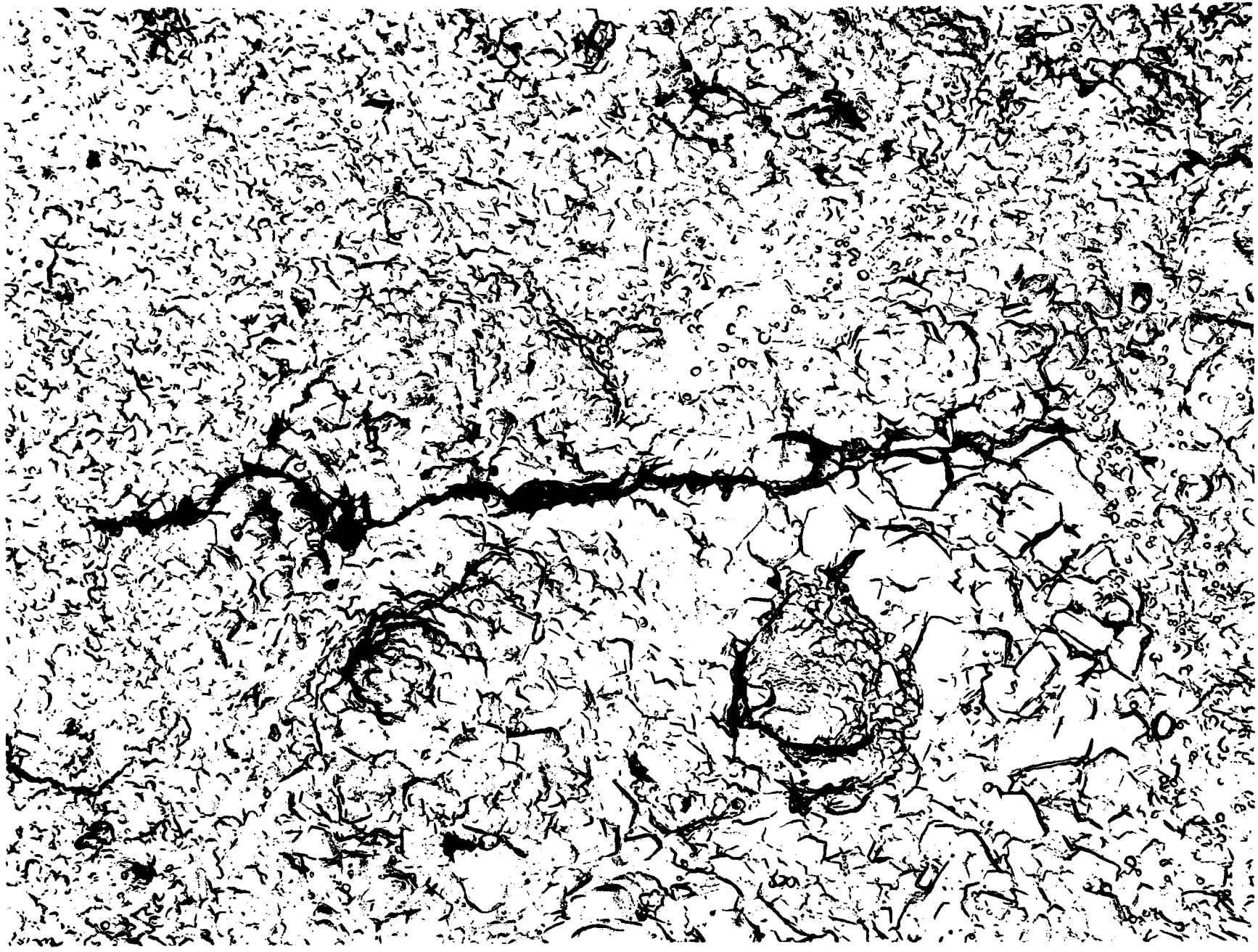


FIGURE 48 Replica Electron Micrograph

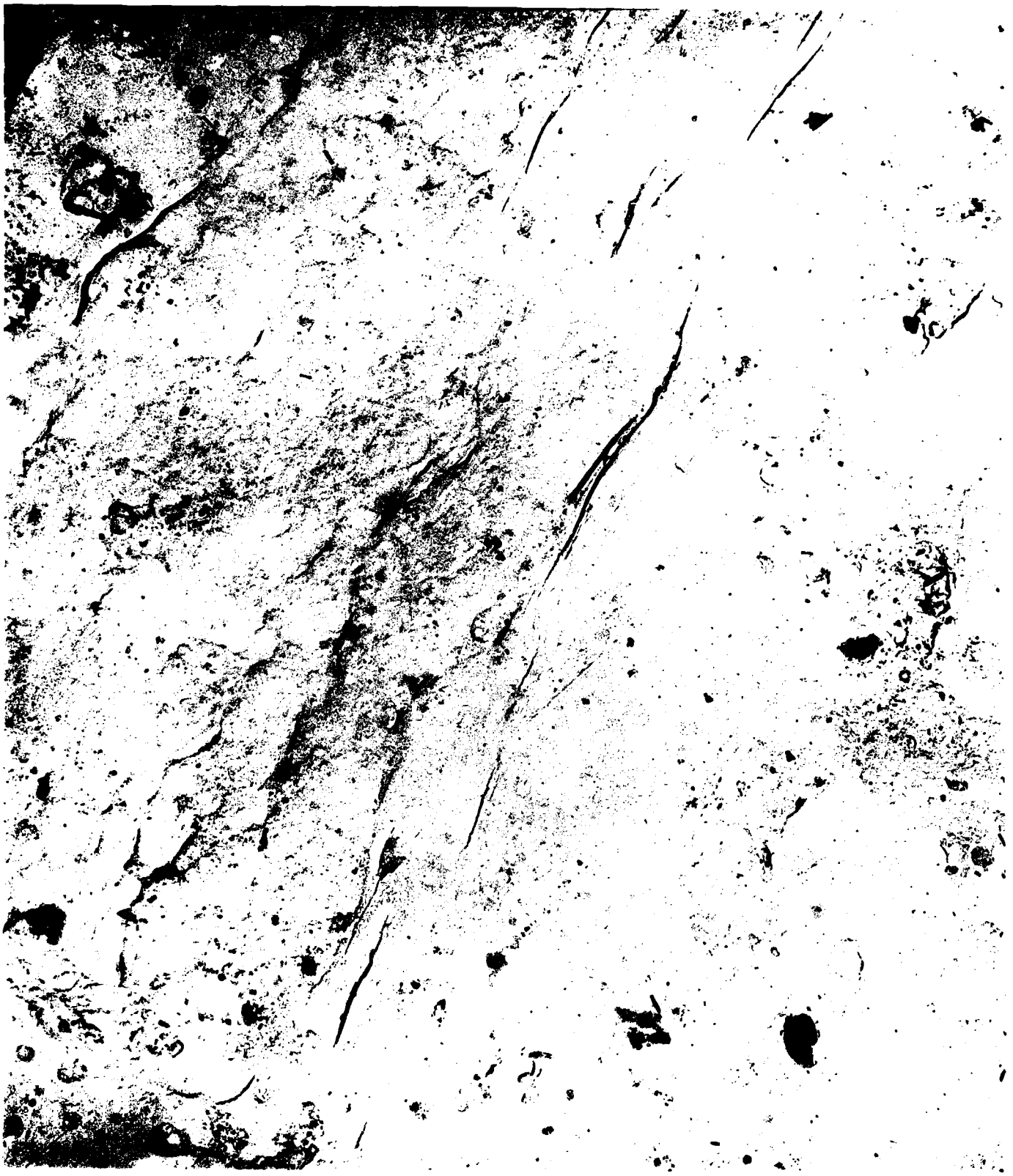


FIGURE 49 Replica Electron Micrograph

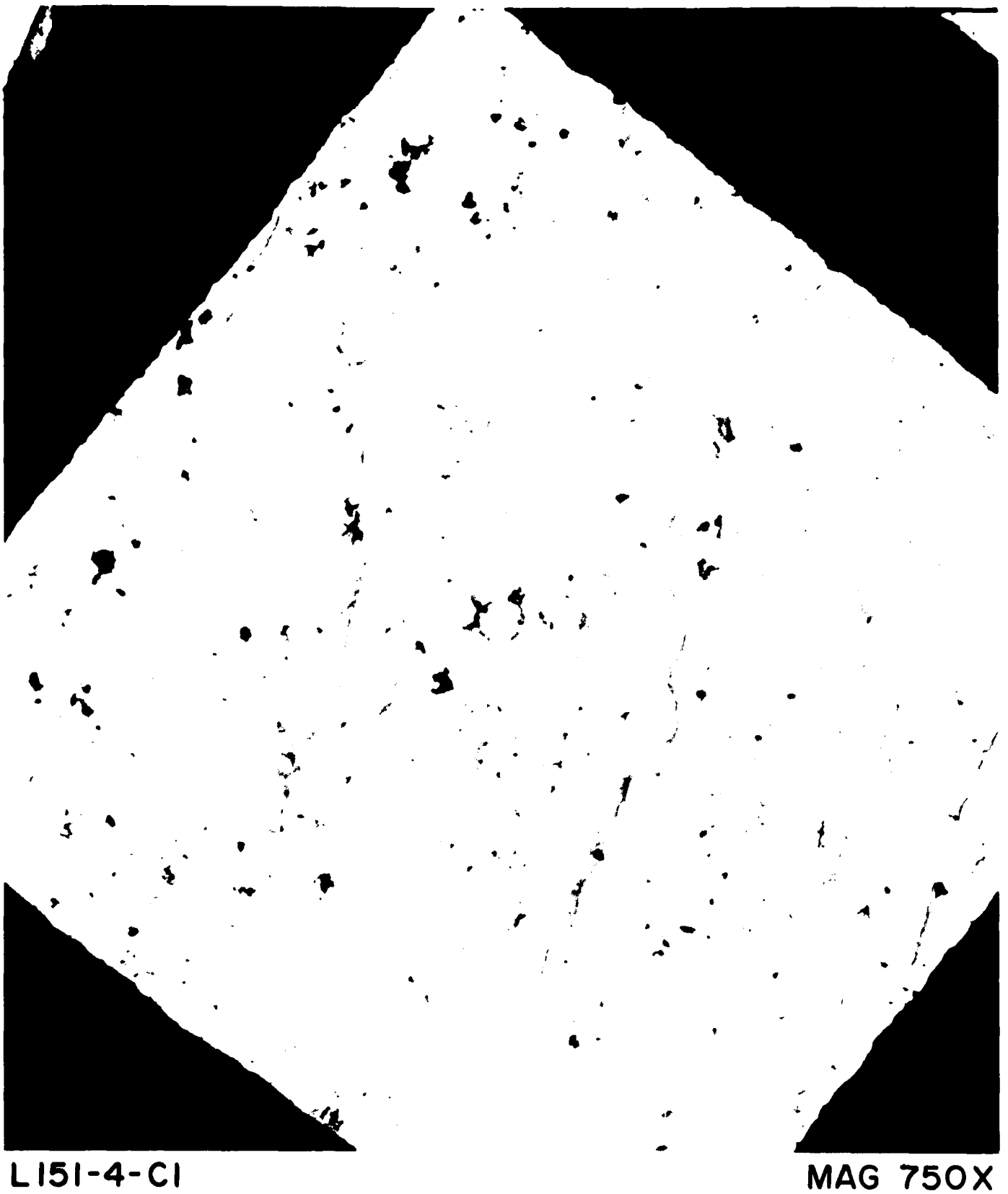


FIGURE 50 Replica Electron Micrograph

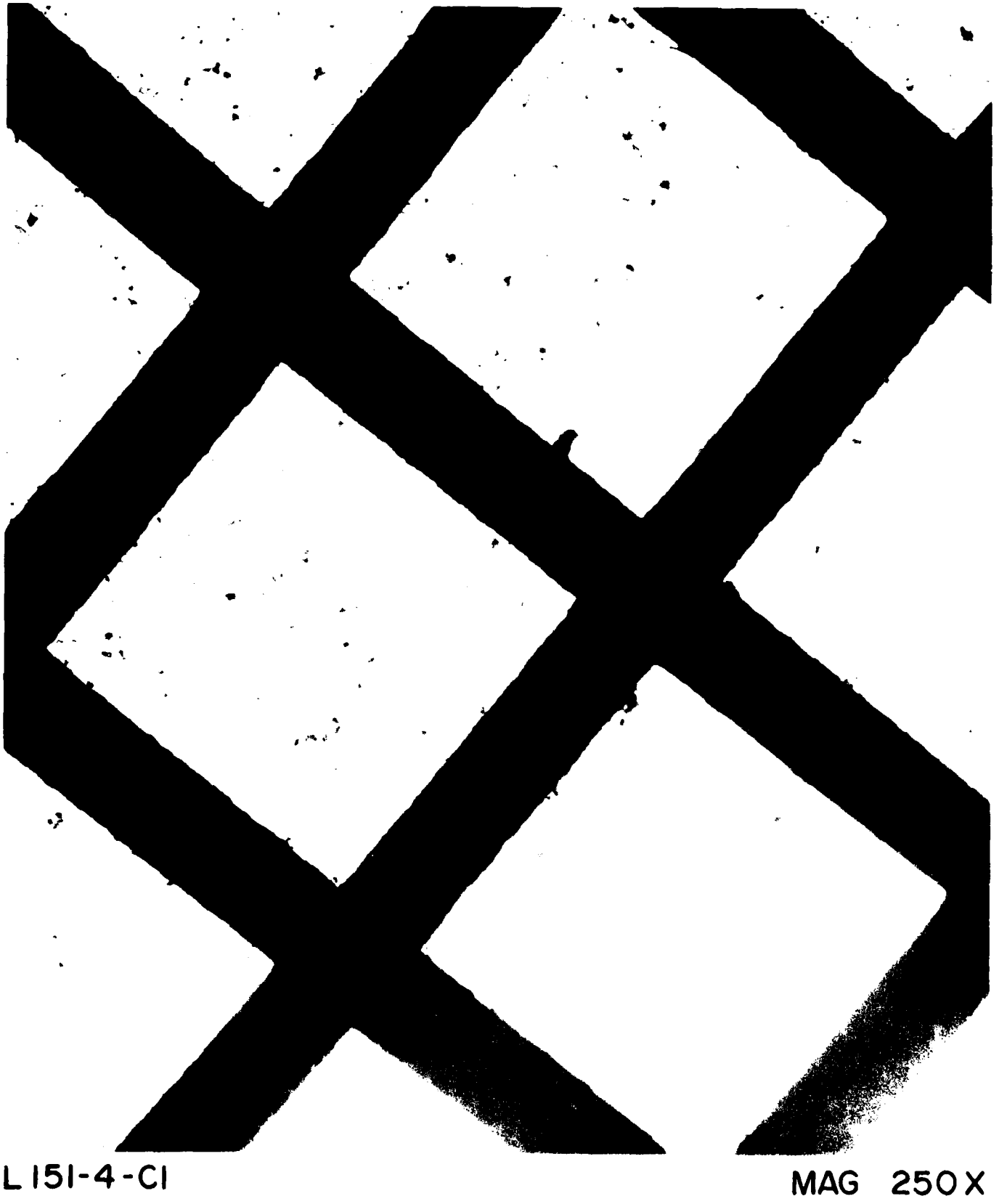


FIGURE 51 Replica Electron Micrograph

END

10-86

DTIC